Soil Biology and Biochemistry 203 (2025) 109735

Contents lists available at ScienceDirect

Soil Biology and Biochemistry

journal homepage: www.elsevier.com/locate/soilbio

Reduction of iron-organic carbon associations shifts net greenhouse gas release after initial permafrost thaw

Eva Voggenreiter [a], Laurel ThomasArrigo [b], Joachim Kilian [c], Daniel Straub [d], Maike Friedel [a], Mark Stahl [c], Andreas Kappler [a,e], Prachi Joshi [a,*]

[a] Geomicrobiology, Department of Geosciences, University of Tuebingen, Schnarrenbergstrasse 94-96, 72076, Tuebingen, Germany
[b] Environmental Chemistry, University of Neuchâtel, Avenue de Bellevaux 51, CH-2000, Neuchâtel, Switzerland
[c] Center for Plant Molecular Biology, University of Tuebingen, Auf d. Morgenstelle 32, 72076, Tuebingen, Germany
[d] Quantitative Biology Center (QBiC), University of Tuebingen, Auf d. Morgenstelle 10, 72076, Tuebingen, Germany
[e] Cluster of Excellence: EXC 2124: Controlling Microbes to Fight Infection, Tuebingen, Germany

ARTICLE INFO

Keywords:
Greenhouse gas emissions
Thaw gradient
Methanogenesis
Mineral-organic carbon interactions
Peat

ABSTRACT

In thawing permafrost soils, associations between organic carbon (OC) and ferric iron (Fe(III)) (oxyhydr)oxide minerals may stabilize OC in recently thawed soil layers, thus limiting the microbially mediated release of greenhouse gases (GHGs) such as carbon dioxide (CO_2) and methane (CH_4). Conversely, the development of anoxic conditions during thaw could lead to the microbial reductive dissolution of these Fe(III)-OC associations, resulting in a mobilization of the associated OC with unknown consequences for GHG release. In this study, we investigated the role of Fe(III)-OC associations (in the form of Fe(III)-OC coprecipitates) in soil GHG release during the collapse of previously oxic permafrost soils ("palsa") and the inundation of seasonally anoxic soils ("bog") at Stordalen Mire (Abisko, Sweden). We performed anoxic microcosm experiments using these two soils with the addition of ^{57}Fe-labeled Fe(III)-OC coprecipitates. The coprecipitates were reduced entirely after 42 days, with rapid reductive dissolution of 22 ± 7% and 20 ± 7% of coprecipitates within 1 day in palsa and bog soils, respectively. Emissions of GHG varied depending on soil type: in case of the palsa soil, cumulative CO_2 emissions increased by 43 ± 16% after addition of the Fe(III)-OC coprecipitates compared to a non-amended control, due to microbial Fe(III) reduction coupled to OC oxidation and likely additional OC input due to the release of Fe-bound OC. Concurrently, we observed an increase in activity of fermenting and complex OC-degrading microorganisms. Within the bog soil, it was notable that CH_4 emissions were temporarily suppressed, likely due to inhibition of methanogenesis by microbial Fe(III) reduction of the added coprecipitates, indicated by a decrease in *mcrA* gene copies. In conclusion, our findings demonstrate that Fe(III)-OC associations do not provide protection for OC after establishment of anoxic conditions during permafrost thaw, with resulting GHG emissions controlled by previous redox status of the soils and the microbial community.

1. Introduction

Thawing permafrost soils are predicted to be an increasing source of the greenhouse gases (GHGs) carbon dioxide (CO_2) and methane (CH_4) due to higher bioavailability of organic carbon (OC) and higher soil temperatures in the future (Schuur et al., 2015). Predicted quantities of released GHGs are uncertain, with estimates varying between 37 and 149 Pg CO_2 and 1090–5050 Tg CH_4 by the year 2100 (Schuur et al., 2022). While most of the emitted OC will be as CO_2, the majority (up to 70%) of the radiative forcing will come from the emission of CH_4, due to its higher global warming potential (28x over a 100 year timescale) (Turetsky et al., 2020; Walter Anthony et al., 2018). The high uncertainty of projected GHG emissions is due to the multifaceted responses of permafrost areas to thaw, varying in hydrologic conditions (Andresen et al., 2020; Sim et al., 2021), soil geochemistry (Ernakovich et al., 2017; Gray et al., 2014) and microbial community composition (Graham et al., 2012; Waldrop et al., 2023). Additionally, the presence of soil minerals, which can bind and presumably stabilize OC against microbial decomposition, is a major factor during permafrost thaw (Gentsch et al., 2018; Lim et al., 2022; Monhonval et al., 2022; Monhonval et al., 2023b)

* Corresponding author.
E-mail address: prachi.joshi@uni-tuebingen.de (P. Joshi).

https://doi.org/10.1016/j.soilbio.2025.109735
Received 15 October 2024; Received in revised form 11 December 2024; Accepted 27 January 2025
Available online 31 January 2025

The fraction of mineral-bound OC in permafrost soils ranges from 33 to 74% of total OC (Gentsch et al., 2015; Liu et al., 2022; Martens et al., 2023; Thomas et al., 2024). The variation of the mineral-bound OC fraction is partly due to different minerals displaying a range of binding capacities for OC, with redox-active ferric iron (Fe(III)) (oxyhydr)oxides contributing to the highest estimates on a mass basis (Hu et al., 2024; Zhu et al., 2023). Interactions of OC with Fe(III) (oxyhydr)oxides can occur due to adsorption to already existing minerals and by coprecipitation of dissolved Fe and OC at oxic-anoxic redox transitions (Kleber et al., 2015), forming Fe(III)-OC associations. Field-based evidence has shown that relatively older OC is stored in mineral fractions of permafrost soils, dominated by Fe(III) (oxyhydr)oxides (Gentsch et al., 2015; Martens et al., 2023), displaying their ability to sequester OC over long time frames. Some studies also demonstrated the preservation or *de novo* formation of Fe(III)-OC associations after permafrost thaw, implying that Fe-bound OC would lead to a lower permafrost-carbon feedback by decreasing future GHG emissions (Liu et al., 2022; Monhonval et al., 2022., 2023a; Thomas et al., 2023). Evidence for the inhibition of permafrost OC degradation due to Fe(III) (oxyhydr)oxides has been given by one study looking at Yedoma permafrost deposits that observed lower basal respiration of thawed sediment layers in correlation with higher amounts of poorly crystalline Fe(III) (oxyhydr)oxides (Martens et al., 2023).

However, the stabilizing function of Fe(III)-OC associations is brought into question if permafrost thaw leads to the development of anoxic conditions due to soil subsidence and waterlogging in lowland permafrost areas (Farquharson et al., 2019; Jorgenson et al., 2013; Varner et al., 2022; Woo and Young, 2006). Anoxic conditions could lead to microbial reductive dissolution of Fe(III) (oxyhydr)oxides, thus releasing the previously bound OC to the aqueous phase (Barreto et al., 2024; Patzner et al., 2020). Although no study has directly investigated the stability of Fe(III)-OC associations in permafrost environments under anoxic conditions, previous work in humid soils may provide useful insights into Fe(III)-OC associations stability and resulting GHG emissions. For example, emissions of CO_2 (Chen et al., 2020) as well as of CH_4 increased (Huang and Hall, 2017) after dissolution of Fe minerals in temperate, agricultural soils, indicating that anoxia might negate Fe-mediated OC protection. Conversely, Fe(III)-OC associations seem to persist in many wetland environments (Sun et al., 2023; Zhao et al., 2023), especially *Sphagnum*-dominated wetlands (Zhao et al., 2023), which typically experience anoxic conditions. Complementarily, it has been demonstrated that Fe(III)-OC associations were reduced to a lower extent than OC-free Fe(III) (oxyhydr)oxides using pure cultures of the Fe (III)-reducing microorganisms of the genus *Geobacter* due to higher particle sizes and limited microbial access to Fe(III) (Eusterhues et al., 2014; Poggenburg et al., 2018). Given this contrasting knowledge, it is unclear what the fate of Fe(III)-OC associations will be after permafrost thaw.

Based on the uncertainty regarding the susceptibility of Fe(III)-OC associations to reduction in thawing permafrost soils, the effect of Fe (III)-OC associations on GHG emissions has not been quantified well. Previous estimates of the contribution of Fe(III) reduction to anaerobic respiration in permafrost soils are based on field measurements of poorly crystalline Fe(III) content and net CO_2 fluxes across thaw transitions (Lipson et al., 2013; Patzner et al., 2022) or after injections of dissolved Fe(III) into the soil (Lipson et al., 2010). Resulting estimates of contributions of Fe(III) reduction to total CO_2 emissions ranged from 22 to 63% (Lipson et al., 2013; Patzner et al., 2022), suggesting that Fe(III) reduction is an important contributor to anaerobic respiration in these soils. However, no conclusions about the direct role of Fe(III)-OC associations on CO_2 release can be drawn based on these measurements. Further, it is unknown how the reduction of Fe(III)-OC associations in thawing permafrost soils would affect net CH_4 release. Previous studies demonstrated the suppression of methanogenesis due to Fe(III) reduction since Fe(III) is a more thermodynamically favorable electron acceptor (Lipson et al., 2012; Miller et al., 2015; Reiche et al., 2008). In contrast, methanogenesis and Fe(III) reduction seemed to occur simultaneously in Alaskan permafrost soils (Herndon et al., 2015; Yang et al., 2016). The release of OC from Fe(III)-OC associations could also increase CH_4 emissions by supplying new OC compounds for fermenting microorganisms which provide the substrates (fatty acids, H_2) for methanogenesis (Drake et al., 2009).

Knowledge of the net effects of Fe(III)-OC associations on GHG emissions during permafrost thaw is, therefore, limited. In this study, we aimed to (i) determine the reduction extent of Fe(III)-OC associations upon permafrost thaw, (ii) quantify the contribution of reduction of Fe (III)-OC associations to GHG release, and (iii) evaluate the changes of microbial community composition due to addition of Fe(III)-OC associations. To achieve this, we synthesized ^{57}Fe-enriched Fe(III)-OC coprecipitates, representative of Fe(III)-OC associations, using water-extractable natural organic matter from a permafrost thaw gradient at Stordalen Mire (Abisko, Sweden). The Fe(III)-OC coprecipitates were then exposed to anoxic conditions in a microcosm experiment containing an anoxic soil slurry from the same site. We performed the experiment using soils of two different permafrost thaw stages. We used intact, oxic permafrost soils ("palsa") and inundated them in order to simulate rapid permafrost thaw, as well as partly thawed permafrost soils ("bog") to simulate the anoxic stage of natural seasonal water table fluctuations. The results of this work will thus help to understand the influence of Fe (III)-OC associations on GHG emissions in thawing permafrost peatlands.

2. Methods

2.1. Field site description and sampling

Stordalen Mire is a well-characterized permafrost peatland complex, located at the edge of the discontinuous permafrost zone near Abisko, Sweden (68 22' N, 19 03' E). It consists of several subhabitats: intact permafrost areas (palsas) covered by dwarf shrubs, bryophytes and lichens, semi-wet bogs dominated by *Sphagnum* spp. mosses, and permanently waterlogged fens covered by sedges (*Eriophorum vaginatum, Carex rostrata*) (Malmer et al., 2005). Mean annual air temperature in Abisko increased from −0.9 °C during 1957–1971 (Malmer et al., 2005) to 0.7 °C during 2005–2019 (Swedish Meteorological and Hydrological Institute, 2020) leading to thawing of permafrost ice underneath palsas and conversion to bog and fen areas (Johansson et al., 2006).

Soil and porewater samples were collected in July 2022. Collected subsoils (30–35 cm depth) from palsa and bog areas were used in the microcosm experiment. The upper soil (2–10 cm depth) was collected and used for extraction of soil organic matter for the Fe(III)-OC coprecipitate synthesis. Both soils were retrieved by bulk sampling and stored in sterilized plastic bags (LDPE). The bog soils, which were fully water saturated, were filled into the bags such that no headspace remained and abiotic oxidation was minimized. Samples were transported under cold conditions via airplane back to Tübingen. In the lab, the soils were stored in gas-tight, N_2-flushed mason jars at 4 °C until use. An aliquot of the soils used for the microcosm experiment was dried (60 °C) inside an anoxic glovebox (MBraun Unilab Workstation, 100% N_2 atmosphere) for initial analysis of Fe speciation by selective extractions (Text S1, Fig. S1) and Fe *K*-edge X-ray absorption spectroscopy (XAS). Total organic carbon content was determined by elemental analysis (SoliTOC Cube, Elementar, Germany). A soil standard was used for calibration (Soil Standard OAS, Cat No B2152, Elemental Microanalysis Limited). Porewater was sampled over different depths (5–43 cm) at four different locations per thaw stage in order to compare *in situ* concentrations of aqueous Fe and OC to results from the microcosm experiments. We used MacroRhizon® samplers (60 cm length, 0.15 μm pore size, Rhizosphere Research, Netherlands) and stored porewater in sterilized serum vials with an N_2 headspace after sampling.

2.2. Synthesis of ^{57}Fe-enriched Fe(III)-OC coprecipitates

A water extraction was used to extract soil organic matter from the upper soils of palsa and bog for the synthesis of Fe(III)-OC coprecipitates. The detailed procedure can be found in Text S2. The final dissolved organic carbon (DOC) concentrations in the extracts (referred to as water-extractable organic matter, WEOM) were 18 and 11 mg C L^{-1} for palsa and bog soil, respectively. The coprecipitates were prepared from an isotopically labeled ^{57}Fe-enriched $FeCl_3$ solution, which made it possible to differentiate added Fe(III)-OC coprecipitates from the native Fe pool. The enriched ^{57}Fe(III) solution (150 mM) was prepared as described previously (Notini et al., 2022; ThomasArrigo et al., 2018) and subsequently mixed with an equimolar $^{NA}FeCl_3$ ($FeCl_3x6H_2O$, Sigma-Aldrich) solution in a ratio of 1:10, to create a 10% ^{57}Fe-enriched Fe(III)Cl_3 solution.

The coprecipitate synthesis involved mixing 1.5 L of the WEOM solution from each thaw stage with the ^{57}Fe-enriched $FeCl_3$ solution to create an initial molar C:Fe ratio of 1. An NaCl solution was added to keep the ionic strength constant (final concentration: 3 mM). The pH was raised by adding 50 mM NaOH dropwise until pH 4.5 under constant stirring (800 rpm). The low pH was chosen since soil pH and porewater pH in palsa and bog soils are between pH 3.5–5.5 (Fig. S2a). The suspensions were left to stand for 2 h, after which the pH was readjusted to pH 4.5. Afterwards, the suspensions were washed by filling them in pre-soaked dialysis membranes (14 kDa, Sigma-Aldrich) in double-deionized (DDI) water. The water was exchanged several times until conductivity was <20 μS cm^{-1}. The washed suspensions were centrifuged, and the solids were resuspended in 50 mL DDI water. The pH was adjusted to pH 4.5 and the solution was bubbled with N_2 (99.999%) for 15 min to make it anoxic. The Fe speciation was characterized by ^{57}Fe Mössbauer spectroscopy (Fig. S3, Table S1) and Fe *K*-edge XAS by X-ray absorption near edge structure (XANES, Fig. S4) and extended X-ray absorption fine structure (EXAFS, Fig. S5). We observed that coprecipitates were made up entirely of Fe(III) (Fig. S4) and consisted of mostly of ferrihydrite (93%) and minor portions of lepidocrocite (7%, Table 1).

2.3. Setup of microcosm experiments

The field-moist subsoils used in the microcosm experiments were homogenized by wet sieving with a sterilized 2 mm sieve. Moist palsa soil (5.5 g dry weight) and bog soil (8 g dry weight) were added to six 250 mL serum bottles each under sterile conditions. The bottles were then closed with sterilized butyl rubber stoppers. The headspace in each bottle was exchanged by applying vacuum for 5 min and flushing with N_2 gas for 5 min (3 cycles). Artificial, anoxic porewater solution (composition in Table S2) was added within an anoxic glovebox to the bottles to reach a final soil-solution ratio of 0.23 and 0.88 mg dry soil mL^{-1} for palsa and bog soil, respectively. All bottles were incubated under anoxic conditions at room temperature (20 °C) in the dark for 30 days prior to the addition of ^{57}Fe-enriched Fe(III)-OC coprecipitates. At this point, coprecipitates that were synthesized using palsa WEOM were added to three of the bottles containing palsa soil, and those synthesized with bog WEOM were added to three bottles containing bog soil. Note that we consider the timepoint right after addition of coprecipitates as day 0. The amount of added ^{57}Fe-enriched Fe(III)-OC coprecipitates was adjusted to the amount of native Fe minerals in each bottle, increasing the total 6 M HCl-extractable Fe by 50% (see Fig. S6d). The remaining bottles contained only either palsa and bog soil, functioning as non-amended controls.

In a control experiment, we tested the importance of abiotic reduction of added Fe(III)-OC coprecipitates by the native DOC within the soil. For that purpose, we added the same concentration of Fe(III)-OC coprecipitates to sterile filtered (0.22 μm, PES, Carl Roth) aqueous phase from the non-amended treatments of palsa and bog soil, collected at the end of the experiment. A new batch of the coprecipitates was prepared for this control experiment in order to have similar storage times as in the main experiment. In the case of the palsa soil, the filtered aqueous phase was diluted with artificial porewater solution in order to have the same concentration of DOC as on day 0 of the main experiment. For bog soil, the DOC was lower at the time of filtration compared to the beginning; thus, the aqueous phase was left undiluted. The speciation of aqueous Fe and concentration of aqueous ^{57}Fe and DOC were quantified over 48 h as specified in section 2.6.

Table 1
Linear combination fitting results for k^3-weighted Fe *K*-edge EXAFS spectra of the initially synthesized ^{57}Fe-enriched Fe-OC coprecipitates and the initial soils, as well as the samples from the microcosm experiment with added coprecipitates ("+cop") and without ("-cop") at day 0, after 1, 8 and 42 days of incubation (labeled as _days). Used references were ferrihydrite, lepidocrocite and various Fe(II)/Fe(III)-OC complexes. The Fe(III)-OC fraction was fit as Fe(III)-citrate and/or Fe(III)-catechol, and the Fe(II)-OC fraction was fit as a combination of Fe(II)-citrate, Fe(II)-catechol and Fe(II)-EDTA.

	sample	Fh[a]	Lp[b]	Fe (III)-OM	Fe (II)-OM	NSSR[c]	red. $\chi^{2,d}$
		[%]	[%]	[%]	[%]	[%]	[-]
Palsa	57FeOC_initial	93	7	0	0	2.3	0.11
	soil initial	29	0	32	39	2.5	0.10
	mix "57FeOC"+"-cop_0"[e]	24	2	20	55	n.a.	n.a.
	+cop_0	16	0	18	66	2.6	0.08
	+cop_1	0	0	26	74	1.7	0.06
	+cop_8	0	0	23	77	1.6	0.05
	+cop_42	0	0	8	93	1.6	0.07
	-cop_0	0	0	26	74	1.8	0.06
	-cop_1	0	0	21	79	2.0	0.07
	-cop_8	0	0	21	80	1.8	0.06
	-cop_42	0	0	15	85	1.8	0.06
Bog	57FeOC_initial	93	7	0	0	1.8	0.09
	soil initial	29	0	23	49	4.3	0.16
	mix "57FeOC"+"-cop_0"[e]	41	2	0	56	n.a.	n.a.
	+cop_0	31	0	0	69	2.4	0.07
	+cop_1	19	0	0	81	4.0	0.13
	+cop_8	16	0	17	68	1.8	0.06
	+cop_42	0	0	18	82	1.4	0.05
	-cop_0	20	0	0	80	5.2	0.16
	-cop_1	21	0	0	79	2.0	0.06
	-cop_8	26	0	0	74	2.5	0.08
	-cop_42	0	0	19	81	1.9	0.06

[a] ferrihydrite.
[b] lepidocrocite.
[c] normalized sum of of squared residuals ($100^* \sum_i (data_i\text{-}fit_i)^2/\sum_i data^2$).
[d] measure of fit accuracy ($((N_{idp}/N_{pts}) \sum_i ((data_i\text{-}fit_i)/\varepsilon_i)^2(N_{idp}\text{-}N_{var})^{-1})$). N_{idp}/N_{pts} and N_{var} are the number of independent points in the model fit (18.1), the total number of data points (181) and the number of fit variables (2–7), respectively.
[e] represents the theoretical Fe speciation according to mixing of the initially synthesized Fe(III)-OC coprecipitates and the non-amended control at day 0 (-cop_0).

2.4. Gas sampling of microcosm experiment

Sampling of the microcosms included measuring GHG fluxes and geochemical sampling inside the glovebox. To measure GHG fluxes, the rubber stoppers of the bottles were pierced with two needles, each attached to a three-way valve. The headspace of all bottles was flushed with moistened N_2 for 10 min via a gas distribution setup. After 10 min, the flow of N_2 gas was stopped and the gases were left to accumulate. A 2 mL sample was taken from the headspace and transferred to a He-flushed 12 mL Exetainer® vial (Labco, UK) after 0, 30 and 60 min. The individual and cumulative gas fluxes were calculated based on the increase in gas concentration (see Text S3).

2.5. Aqueous and solid phase sampling of the microcosm experiment

The geochemical sampling was carried out in an anoxic glovebox. An aliquot of the suspension (1 mL before addition of Fe(III)-OC coprecipitates, 1.5 mL during the main experiment) was taken out using a needle and syringe. The suspension was centrifuged (10055 rcf, 5 min) and the supernatant was pipetted off. The supernatant was used to quantify DOC concentration and aqueous Fe speciation after acidification with anoxic 1 M HCl. The soil pellet was dried at 60 °C in anoxic conditions overnight and weighed to estimate the dry mass in each sample. The poorly crystalline Fe mineral fraction was quantified by adding 1.5 mL anoxic 0.5 M HCl to the dried soil (Heron et al., 1994; Kostka and Luther, 1994). After 24 h, the extraction solution and remaining solid were separated by centrifugation (10055 rcf, 5 min) and the supernatant was diluted in 1 M HCl for measurement of Fe speciation and ^{57}Fe concentration.

At certain time points (day 0, after 8 and 42 d) an additional 15 mL of suspension was taken out of the bottles. An aliquot (4 mL) was centrifuged in the glovebox, the supernatant was transferred to a new tube and immediately frozen (−20 °C) for measurement of microbial metabolites by gas chromatography mass spectrometry (GC-MS). The soil pellet was frozen (−20 °C) and subsequently freeze-dried under anoxic conditions for analysis by Fe *K*-edge XAS. A separate aliquot of 1 mL was used to measure pH (InLab Easy BNC, Mettler Toledo, Germany) outside the glovebox. The remaining 10 mL were transferred to 15 mL centrifuge tubes (polypropylene, RNase- and DNase-free, Biologix) and centrifuged outside the glovebox (17200 rcf, 5 min). The supernatant was pipetted off under sterile conditions and the remaining soil pellet was immediately frozen (−80 °C) for later extraction of DNA and RNA and subsequent molecular biological analysis (see section 2.8).

2.6. Geochemical analysis

DOC concentrations were measured (as non-purgeable OC) after acidification with 2 M HCl by a TOC analyzer (multi N/C 2100S, Analytik Jena AG, Germany). Aqueous Fe speciation and total aqueous Fe concentrations, as well as the Fe speciation and concentration of the 0.5 M HCl extracts (solid-phase Fe) were quantified using the ferrozine assay (Stookey, 1970). No ferric Fe was detected in the aqueous Fe pool, thus we refer to aqueous Fe concentrations later as aqueous Fe^{2+} concentrations. We only interpreted changes of total Fe concentrations from the solids and not its speciation since abiotic reduction of Fe(III) by OC under acidic conditions leads to an underestimate of the Fe(III) content (Chen et al., 2003; Lau et al., 2015).

Gas samples were measured by a gas chromatograph (TraceGC1300, ThermoFisher Scientific, USA; modified by S + HA analytics), equipped with two column configurations (first configuration: 30 m long, 0.53 mm ID TGBondQ column and 30 m long, 0.53 mm ID Molsieve column; second configuration: 30 m long, 0.53 mm ID TGBondQ column and a 30 m long 0.25 mm ID TGBondQ + column; all ThermoFisher Scientific) which are each connected to a Pulse Discharged Detector. Gas concentrations were quantified with external calibrations of standards of pure CH_4 and CO_2 (99.5% CH_4, 99.9% CO_2, Westfalen) in He-flushed Exetainer® vials in a range of 0.05–500 ppm.

Concentrations of ^{57}Fe in aqueous and 0.5 M HCl-extracted solid samples were quantified by inductively coupled plasma mass spectrometry (ICP-MS, Agilent 7900, Agilent Technologies, USA) with Ar as carrier gas and in He mode after dilution in 1% HNO_3 (analytical grade, Carl Roth). Contribution of ^{57}Fe-enriched Fe-OC coprecipitates to the aqueous and solid (0.5 M HCl-extractable) Fe pool were calculated (Text S4). The concentration of microbial organic metabolites, such as small sugars, organic acids, and amino acids were quantified using targeted GC-MS (Shimadzu GC/MS TQ 8040, Japan). A full list of measured metabolites is given in Table S3. Metabolites were analysed either by headspace injection or as liquid samples after derivatization and addition of octanol or ^{13}C-glucose as internal standard, respectively (details in Text S5). Concentrations were quantified with an 8-point external calibration containing standards of all targeted analytes, ranging from 20 to 10^7 pmol.

2.7. Solid phase Fe characterization

Iron speciation in the solid was investigated by Fe *K*-edge XAS at Synchrotron SOLEIL (SAMBA beamline, Gif-sur-Yvette, France) and Synchrotron ELETTRA (XAFS beamline, Trieste, Italy). For this purpose, the initial ^{57}Fe-enriched coprecipitates were air-dried prior to homogenization with a mortar and pestle. The dried solids were pressed into pellets (7 mm diameter) with PVP (Polyvinylpyrrolidone K12, Carl Roth) and sealed with Kapton® tape. Freeze-dried samples of solids from the microcosms were processed in the same way in a glovebox after anoxic freeze drying (see section 2.5 above).

At both beamlines, transmission spectra were recorded at 77 K using a N_2(l) cryostat. At SOLEIL, a Si(220) monochromator was used and calibrated to the first derivative maximum of the *K*-edge absorption of an Fe(0) foil. Harmonic rejection was performed by two Si mirrors coated in Pd. Between 8 and 14 scans per sample were collected in continuous scan mode and merged. At ELETTRA, an Si(111) monochromator was calibrated to the first derivative maximum of the *K*-edge absorption spectrum of an Fe(0) foil. Higher beam harmonics were decreased by detuning the monochromator by 30%. Two to three scans were collected per sample and merged. The merged spectra were used for analysis of Fe *K*-edge XANES to estimate Fe oxidation state and EXAFS to determine Fe speciation through linear combination fitting. All data processing and analysis were done in Athena software (Ravel and Newville, 2005) with detailed description included in Text S6. The initial synthesized ^{57}Fe-enriched Fe(III)-OC coprecipitates were analysed using ^{57}Fe Mössbauer spectroscopy to determine Fe speciation. Details on the measurement and data analysis are given in Text S7.

2.8. Molecular biology analysis

Total DNA and RNA of soil samples from the microcosm experiment were extracted in experimental triplicate using the RNeasy PowerSoil® Total RNA Kit with DNA Elution (Qiagen, Germany). Details on protocol adjustments, quality control steps and transformation of RNA to cDNA are given in Text S8. Bacterial and archaeal 16S rRNA genes were amplified from DNA and cDNA using the universal primers 515f (Parada et al., 2016) and 806r (Apprill et al., 2015) fused to Illumina adapters. Library preparation steps (Nextera, Illumina) and sequencing were performed using Illumina MiSeq sequencing system (Illumina, USA) at the Institute for Medical Microbiology and Hygiene of the University of Tübingen. Data processing, including quality control, reconstruction of sequences and taxonomic annotation (Text S8) was done using nf-core/ampliseq version 2.8.0 (Straub et al., 2020; Straub et al., 2024) of the nf-core collection of workflows (Ewels et al., 2020).Fe(III)-reducing, Fe(II)-oxidizing as well as methanotrophic and methanogenic microorganisms were identified, as listed elsewhere (Patzner et al., 2022 and references therein). To evaluate which microbial taxa were significantly affected by addition of Fe(III)-OC coprecipitates, we used the multivariate analysis of composition of microbiomes (ANCOM) (Mandal et al., 2015). We compared the relative abundance of all ASVs in DNA- and RNA-based datasets after 8 and 42 days of the coprecipitate-amended treatment to the non-amended control, since we expected only minimal changes at day 0.

Quantitative PCR (qPCR) was performed on DNA and cDNA samples to quantify changes in total bacterial and archaeal 16S rRNA (gene) copies as well as for methyl-coenzyme M reductase subunit alpha (*mcrA*), a functional gene relevant for CH_4 production (Friedrich, 2005; Juottonen et al., 2006). The used primer sequences, plasmid standards, dilution factors of samples and details of the temperature programs are summarized in Table S4. The assays were performed using SybrGreen® Supermix (Bio-Rad Laboratories, USA) on the C1000 Touch thermal

cycler (CFX96TM real time system, Bio-Rad Laboratories). Sample dilutions (10-1000x) were necessary since presence of complex OC compounds lead to inhibition of the fluorescence signal in samples with no dilution (Winkel et al., 2018). Copy numbers were determined in analytical triplicate of each experimental replicate. Data analysis was performed in Bio-Rad CFX Maestro 1.1 software, vs. 4.1 (Bio-Rad, 2017).

2.9. Statistics

Mean and standard deviations were calculated for each variable analysed in triplicate. When differences between treatments with added Fe(III)-OC coprecipitates and the non-amended controls were calculated, the mean values were used for calculation and the errors (standard deviation) were propagated. Datasets involving GHG fluxes, concentrations of microbial metabolites, relative abundances of taxa on the phyla level of the microbial community and qPCR-based copy numbers were compared between the coprecipitate-amended and non-amended treatments using a two-way ANOVA, followed by Tukey HSD tests. If datasets were non-parametric, they were log transformed unless otherwise stated. All statistical analyses were performed in R version 4.3.3 (R Core Team, 2024).

3. Results

3.1. Aqueous Fe speciation in palsa and bog soils

Aqueous Fe^{2+} concentrations in microcosms were quantified in order to track the reductive dissolution of added ^{57}Fe-enriched Fe(III)-OC coprecipitates in palsa and bog soils. During the initial incubation stage before the addition of Fe(III)-OC coprecipitates, both soils exhibited an increase in aqueous Fe^{2+} concentrations over time which plateaued at 48 ± 1.1 μmol Fe^{2+} g^{-1} soil after 30 days in the palsa microcosm and at 24 ± 0.3 μmol Fe^{2+} g^{-1} soil after 14 days in the bog microcosm (Fig. S6a). The aqueous Fe^{2+} concentrations at the start of the experiment (equivalent to 0.16 ± 0.02 and 0.58 ± 0.09 mM Fe^{2+} in the palsa and bog reactors, respectively, Fig. S6b) were consistent with the concentrations measured in the porewater taken from the field site (Fig. S2b). In the field, we observed increasing Fe^{2+} concentrations with depth (Fig. S2b).

After addition of the coprecipitates, there was an increase in aqueous Fe^{2+} concentrations in coprecipitate-amended treatments compared to the non-amended controls (ΔFe_{aq}). After one day, ΔFe_{aq} was 7.44 ± 4.52 μmol Fe^{2+} g^{-1} soil in palsa soil and 9.66 ± 0.50 μmol Fe^{2+} g^{-1} soil in bog soil (Fig. 1a and b). This difference stayed constant for the duration of the experiment, fluctuating around 10.10 ± 3.16 and 11.00 ± 3.72 μmol Fe^{2+} g^{-1} soil for palsa and bog soil, respectively. Based on ΔFe_{aq} between the two treatments, 22 ± 7% and 20 ± 7% of added Fe (III) in coprecipitates were dissolved in palsa and bog soil, respectively. To directly quantify aqueous Fe from the added Fe(III)-OC coprecipitates, we measured ^{57}Fe concentrations (Fig. 1c and d). This dataset also showed an increase in aqueous Fe from the coprecipitates in coprecipitate-amended treatments to 14.45 ± 2.16 and 6.84 ± 0.50 μmol Fe g^{-1} soil for palsa and bog soil, respectively, after one day. The dissolution of coprecipitates based on the aqueous ^{57}Fe dataset was 32 ± 5% and 12 ± 1% for palsa and bog coprecipitates, respectively.

3.2. Solid phase Fe speciation in palsa and bog soils

We determined changes in solid phase Fe speciation in the microcosms over time by using Fe *K*-edge XAS. The fraction of oxidized Fe (Fe

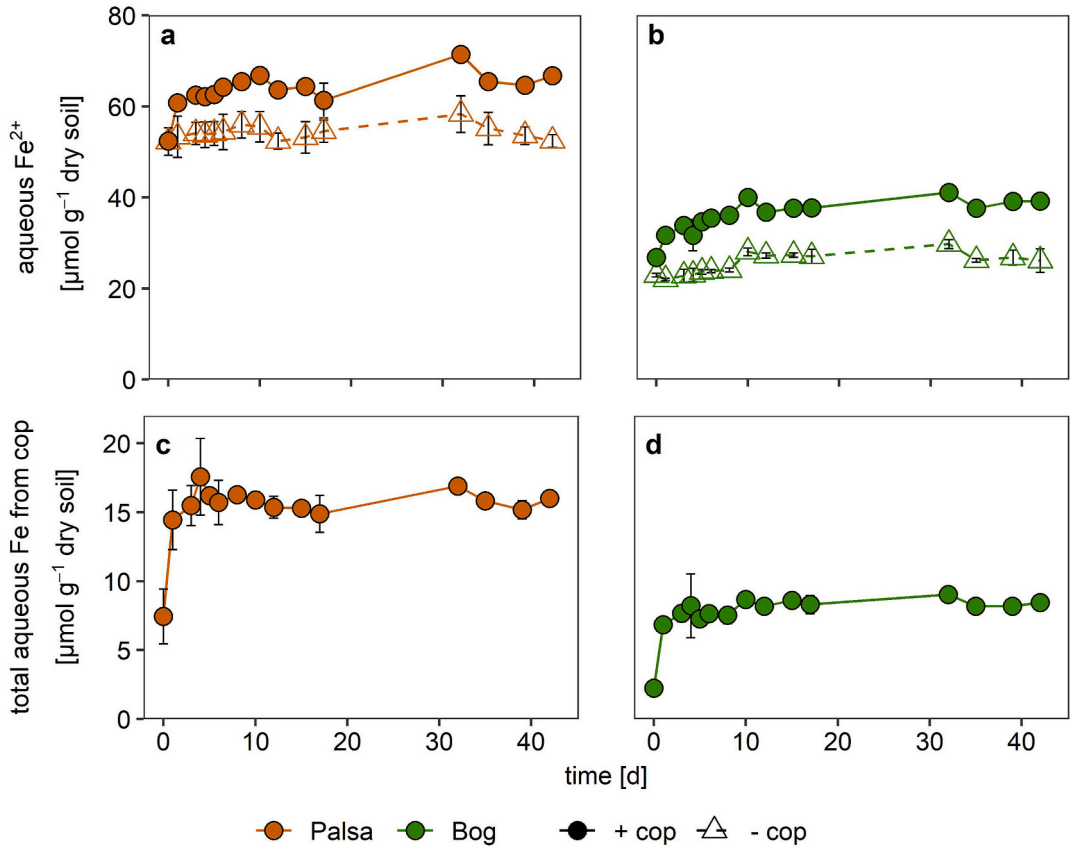

Fig. 1. Concentrations of aqueous Fe [μmol g^{-1} dry soil] over time. Measured concentrations of aqueous Fe^{2+} in treatments with Fe(III)-OC coprecipitate addition ("+ cop", filled circles) and the non-amended control ("- cop", open triangles) of palsa and bog soils (a–b). Calculated concentrations of aqueous Fe stemming from Fe (III)-OC coprecipitates based on the fraction of ^{57}Fe (c–d). All data points and error bars represent the average and standard deviation of experimental triplicates.

(III)/total Fe) in the solid phase based on XANES fitting decreased over time in the microcosm experiment in both soils (Fig. 2a, Table S5). At day 0, the fraction of Fe(III) in both soils without added coprecipitates was similar (20 and 18% in palsa and bog soil, respectively). In the coprecipitate-amended treatments, the fraction was higher by 8% and 13% than in the non-amended control for palsa and bog soil, respectively. Based on the mass of added total Fe (estimated from 0.5 M HCl extraction, Fig. S6d), the addition of Fe(III)-OC coprecipitates, all of which was initially Fe(III) (Fig. S4), initially contributed to 30% of total Fe in the coprecipitate-amended reactors. After one day of incubation, the fraction of Fe(III) in coprecipitate-amended treatments decreased further and the difference in fraction of Fe(III) between the coprecipitate-amended and non-amended control treatment only made up 3% and 2% for palsa and bog soil, respectively. In the palsa soil, the fraction of Fe(III) in both treatments continued to decrease until the end of the experiment (42 days), after which no Fe(III) was present in the coprecipitate-amended treatment and 7% Fe(III) was in the non-amended control. In the bog soil, the percentage of oxidized Fe slightly increased in both treatments after 8 days, after which it decreased again to 10 and 13% for the coprecipitate-amended and non-amended treatment, respectively, at the end of the experiment (42 days).

The relative abundances of the two identified Fe(III) phases, ferrihydrite and Fe(III) directly bound to OC (Fe(III)-OC), varied over time (Fig. 2b). We detected a higher percentage of ferrihydrite in the coprecipitate-amended treatments compared to the non-amended controls at day 0 for both soils (16% compared to 0% and 31% compared to 20% for palsa and bog soil, respectively), which is consistent with the primary Fe phase in the coprecipitates being ferrihydrite (section 2.2). The fraction of ferrihydrite in the coprecipitate-amended treatment decreased in both soils and reached 0% after 1 day in palsa soil and after 42 days in the bog soil. Concurrently, the percentage of Fe(III)-OC (initially) increased in the coprecipitate-amended treatment of both soils. In the palsa soil, the fraction of Fe(III)-OC increased from 18% to 26% within 1 day, before decreasing to 8% at day 42. In the bog soil, Fe (III)-OC increased from 0% to 17% within 8 days and stayed constant for the remaining experiment. While Fe(III) phases decreased, the percentage of Fe(II) bound to OC (Fe(II)-OC) increased in all treatments (Table 1).

3.3. Greenhouse gas emissions in palsa and bog soils

The impact of the coprecipitate addition on the release of GHGs varied depending on the soil type. In palsa soils, cumulative CO_2 emissions significantly increased in the coprecipitate-amended treatment compared to the non-amended control by 43 ± 16% (733 ± 80 compared to 511 ± 15 μmol CO_2 g^{-1} soil, ANOVA, $p < 0.01$) over 42 days (Fig. 3a). After 3 days, the CO_2 fluxes of the coprecipitate-amended palsa treatment were higher than the respective control and showed the largest difference after 10 and 12 days (ANOVA, $p < 0.05$, Fig. S7). In contrast, cumulative CO_2 emissions did not differ between the two treatments in the bog soil (535 ± 22 compared to 523 ± 38 μmol CO_2 g^{-1} soil in coprecipitate-amended and control treatment, respectively) after 42 days. Also, individual CO_2 fluxes between the two bog treatments were not significantly different from each other at any timepoint.

Emissions of CH_4 were below the detection limit in both treatments for the palsa soil during the entire experiment (Fig. 3b). In contrast, continued CH_4 emissions were detected in both treatments of the bog soil and cumulative emissions at the end of the experiment did not differ from each other (273 ± 7.6 compared to 251 ± 62 μmol CH_4 g^{-1} soil for coprecipitate-amended and non-amended treatment, respectively). In the beginning of the experiment, cumulative CH_4 emissions were slightly lower from day 0 to day 12 in the coprecipitate-amended treatment compared to the non-amended control (15 ± 8.9 compared to 22 ± 12 μmol CH_4 g^{-1} soil, Kruskal-Wallis test, $p = 0.18$).

3.4. Shifts in microbial community in palsa and bog soils

Changes in microbial community composition and potential activity upon addition of Fe(III)-OC coprecipitates were monitored using 16S rRNA (gene) amplicon sequencing and quantification of the bacterial and archaeal 16S rRNA gene over the course of the microcosm experiment. Community composition differed between the two soils and changed over time. Within the palsa soil, the community was dominated by the phyla *Acidobacteriota, Actinobacteriota, Proteobacteria* and *Firmicutes*. The RNA-based relative abundance of the phylum *Acidobacteriota* increased over time for both treatments of the palsa soil (44 ± 3% at day 0 compared to 62 ± 6% at day 42, Fig. 4a). After 42 days of incubation, there was a significantly higher relative RNA-based abundance of *Firmicutes* in the coprecipitate-amended palsa treatment compared to the

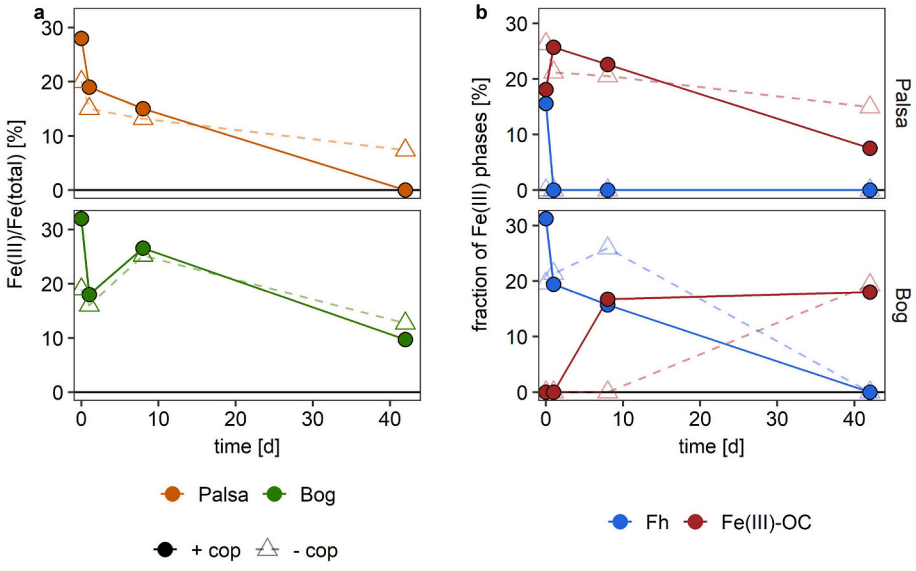

Fig. 2. Solid phase Fe speciation of palsa (upper panel) and bog soil (lower panel) in microcosm experiment with addition of ^{57}Fe-enriched Fe(III)-OC coprecipitates (+cop, filled circles) and without (-cop, open triangles). The Fe(III)/Fe(total) ratio based on linear combination fitting of Fe *K*-edge XANES region for soil is displayed over time (a). The fraction of Fe(III)-containing phases, ferrihydrite (Fh) and Fe(III)-OC phases (Fe(III)-OC), based on linear combination fitting of k^3-weighted Fe *K*-edge EXAFS spectra is shown over time (b).

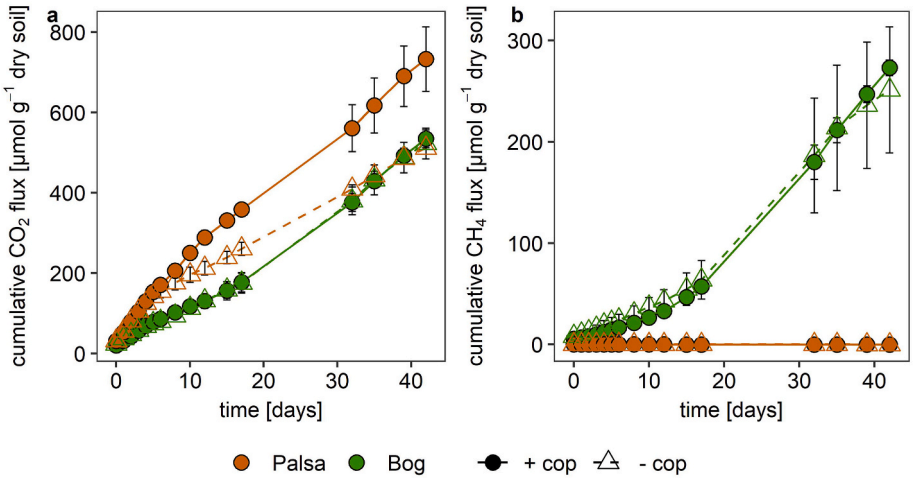

Fig. 3. Cumulative greenhouse gas emissions of CO_2 (a) and CH_4 (b) in microcosm experiments of palsa and bog soils with addition of ^{57}Fe-enriched Fe(III)-OC coprecipitates ("+ cop") and in a non-amended control ("- cop") over time. All data points and error bars represent the average and standard deviation of experimental triplicates respectively.

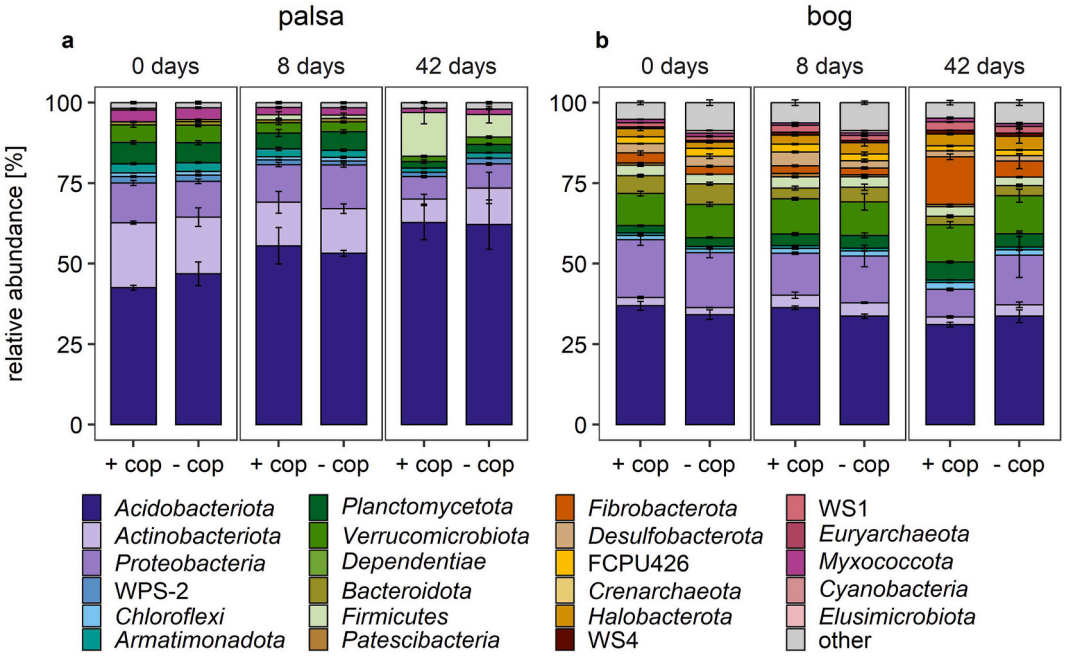

Fig. 4. Shifts in the likely active (RNA-based) microbial community of palsa (a) and bog (b) soil in microcosm experiment with addition of ^{57}Fe-enriched Fe(III)-OC coprecipitates ("+ cop") and in a non-amended control ("- cop") over time. Taxa are displayed at the phylum level and those with a relative abundance below 0.5% were categorized as "other". Data and error bars represent average and standard deviation of experimental triplicates. The DNA-based dataset shows similar trends and is displayed in Fig. S13.

respective non-amended control (14 ± 3% compared to 7 ± 3%, two-way ANOVA, $p < 0.01$). Additionally, ANCOM revealed that the abundance of *Sphingomonas* spp. was significantly higher in the coprecipitate-amended treatment of DNA- and RNA-based samples after 8 and 42 days compared to the non-amended control. Based on qPCR results, RNA-based gene copy numbers of bacterial and archaeal 16S rRNA gene were higher in the coprecipitate-amended palsa soil directly after addition of coprecipitates at day 0 compared to the non-amended control (log_2 FC: 1.44 ± 0.58 and 1.29 ± 0.69, respectively, Fig. S8).

The microbial community in the bog soil was more diverse than in the palsa soil, based on the number of phyla present. The dominant phylum was *Acidobacteria*, similar to the palsa soils, but its relative abundance did not change over time; instead, it remained constant at 34 ± 2% (Fig. 4b). It was also notable that the relative abundance of *Fibrobacterota* significantly increased in the coprecipitate-amended bog treatment compared to the respective non-amended control after 42 days (15 ± 1% compared to 5 ± 2%, two-way ANOVA, $p < 0.001$). Upregulated taxa due to coprecipitate addition based on ANCOM also included *Sphingomonas*, as well as *Geobacteraceae* (full list given in Fig. S9). Copy numbers of the bacterial and archaeal 16S gene in the coprecipitate-amended bog treatment did not differ from the non-amended control over time (Fig. S8), contrary to the palsa treatments.

The abundance and activity of methane-metabolizing microorganisms was determined by identifying taxa known as methanogens and methanotrophs based on 16S rRNA (gene) amplicon sequencing and quantifying *mcrA* gene copy numbers across the experiment. We detected no known genera of methanogens in the palsa treatments at any timepoint of the incubation (Fig. S10). This is consistent with the

findings of the *mcrA* gene copy numbers. DNA-based *mcrA* copy numbers in the palsa treatments were ca. 100 times lower than for the bog treatments and did not change between the coprecipitate-amended and the non-amended control (Fig. S11). RNA-based copy numbers of *mcrA* were below detection limit within the palsa soil. In comparison, a few aerobic methanotrophs were detected (*Roseiarcus*, *Methylocapsa*, *Rhodoblastus*) and their relative abundance decreased over time regardless of the treatment (0.68 ± 0.05% at day 0 compared to 0.26 ± 0.06% at day 42, Fig. S10).

In the bog treatments, we detected a few taxa known as methanogens: *Bathyarchaeia*, *Methanosarcina*, *Methanobacterium* and *Methanomassiliicoccales*. The RNA-based relative abundance of all methanogens increased more in the non-amended treatment over time than it did for the coprecipitate-amended treatment (from 2.41 ± 0.29% to 4.81 ± 2.14% compared to 3.00 ± 0.59% to 4.23 ± 0.31%, Fig. S10). The largest difference between the relative abundance of the two treatments was after 8 days of incubation (0.77 ± 1.14% difference), particularly driven by changes in relative abundance of *Methanosarcina*. Concurrently, DNA-based *mcrA* copy numbers were lower in the coprecipitate-amended treatment after 8 days compared to the non-amended control ($\log_2$ fold change (FC): −0.31 ± 0.14, Fig. 5) while copy numbers did not differ based on treatment after 42 days ($\log_2$ FC: −0.01 ± 0.50). On the other hand, RNA-based *mcrA* copy numbers did not differ significantly from the non-amended control after 8 days and instead were slightly lower after 42 days ($\log_2$ FC: −0.64 ± 0.39). The trends in DNA-based relative abundances of methanogens and methanotrophs were similar to the RNA-based results (Fig. S10).

4. Discussion

4.1. Fe(III)-OC coprecipitates are readily reduced in thawing permafrost soils

The results overall show that Fe(III)-OC coprecipitates were fully reduced in thawing permafrost soils once anoxic conditions develop. Both datasets based on ΔFe_{aq} and aqueous ^{57}Fe concentrations show that there was rapid reductive dissolution of added Fe(III)-OC coprecipitates in both soils (Fig. 1). Results of the ^{57}Fe-based analysis were similar compared to the ΔFe_{aq} values. In case of the palsa microcosms, it is likely that this difference was a consequence of partial abiotic Fe isotope exchange, further discussed below.

Based on the aqueous ^{57}Fe concentrations, all of the reductive dissolution of added Fe(III)-OC coprecipitates occurred within one day and did not change further along the incubation. We considered the following explanations: first, it is possible that there was abiotic reduction of Fe(III) in the coprecipitates due to complexation with redox-active DOC at the low pH (palsa: pH 3.4–3.8, bog: pH 4.2–4.7, Fig. S6i) in the microcosms. Especially aromatic and (poly-)phenolic organic carbon functional groups are known to reduce Fe(III) abiotically at low pH (Chen et al., 2003). We tested this possibility with an abiotic experiment in which the same concentration of coprecipitates was added to sterile-filtered aqueous phase from the control treatment (see section 2.3). We did not observe any increase in aqueous Fe^{2+} concentrations over 48 h, indicating that no abiotic reduction of Fe(III) in coprecipitates by the native DOC occurred. Instead, coprecipitate-amended treatments of palsa and bog soils showed an immediate decrease of aqueous Fe^{2+} compared to the reactors without addition of coprecipitates (6% and 8% respectively, Fig. S12). After 48 h, there was no further change in aqueous Fe^{2+} or total Fe concentration in any of the reactors. The decrease is therefore attributable to sorption of native aqueous Fe^{2+} onto the coprecipitate surface which has been shown before for aqueous Fe^{2+} and naturally occurring Fe(III)-OC coprecipitates from a wetland (ThomasArrigo et al., 2017), as well as for synthesized Fe(III) (oxyhydr)oxides (Pedersen et al., 2005; Williams and Scherer, 2004).

This abiotic experiment also enabled us to test if abiotic isotope exchange between the ^{57}Fe(III) in coprecipitates and the aqueous $^{56}Fe^{2+}$ was responsible for the entire change in aqueous Fe isotopic composition in the main experiment. The fraction of aqueous ^{57}Fe in the abiotic experiment increased by 1.86 ± 0.02% and 1.21 ± 0.03% within 48 h in the coprecipitate-amended treatment of palsa and bog reactors, respectively, compared to the non-amended control (Fig. S12). The change in the aqueous ^{57}Fe fraction was therefore smaller than in the main experiment (2.23 ± 0.19% and 2.37 ± 0.17% in palsa and bog reactors, respectively). Coupled with the fact that aqueous Fe^{2+} and aqueous total Fe concentrations did not increase in the abiotic experiment, this dataset therefore shows that abiotic isotope exchange cannot explain the full increase of aqueous ^{57}Fe that we observed within two

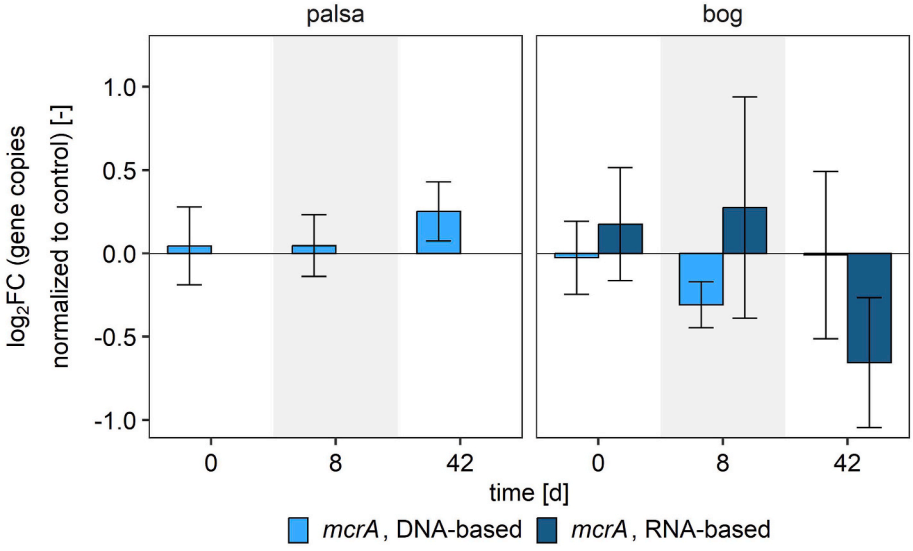

Fig. 5. Change in copy numbers of the *mcrA* gene in microcosm experiment of palsa and bog soils with added ^{57}Fe-enriched Fe(III)-OC coprecipitates based on quantitative PCR results. Results are displayed as the $\log_2$ fold change (FC) of the mean copy numbers of "+ cop" treatment to the mean of the non-amended control [copies $_{+\ cop}$ g^{-1} dry soil/copies$_{-cop}$ g^{-1} dry soil] for DNA- and RNA-based analysis per time point. RNA-based *mcrA* gene copies in the palsa soil were below the detection limit. Absolute gene copy numbers are displayed in Fig. S12. Data bars and error bars represent the mean and 95% confidence interval of experimental triplicates, respectively.

days in the main experiment. The isotopic exchange is likely the reason why the extent of reductive dissolution of coprecipitates in the palsa soil based on ^{57}Fe concentrations and aqueous Fe^{2+} concentrations did not match.

The second possibility that would explain the rapid reductive dissolution of added coprecipitates is that the microbial community was well adapted to the reduction of Fe(III)-OC associations. We found several taxa which are known as respiratory (*Geobacter*, *Pseudomonas, Anaeromyxobacter*) and fermentative (*Clostridiales*) Fe(III)-reducers (Coates et al., 1996; Li et al., 2017; Lovley et al., 2004; Treude et al., 2003), which could play a role even if their total relative abundance did not exceed 1% (Fig. S13). Other yet unidentified Fe(III)-reducing microorganisms, possibly within the phyla *Acidobacteriota* or *Firmicutes* (Blöthe et al., 2008; Glodowska et al., 2021; Hultman et al., 2015; Li et al., 2011) could have also contributed to Fe(III) reduction of the coprecipitates.

We also considered a third possibility that soil-derived, reduced particulate organic matter (POM) could have transferred electrons to the Fe(III)-OC coprecipitates, either abiotically, as shown with dissolved, redox-active DOC (Bauer and Kappler, 2009) or biotically by microorganisms using the POM as an electron shuttle (Roden et al., 2010). Assuming that POM can transfer 0.08 mmol e^- g^{-1} POM in its reduced state, as estimated in Swedish non-permafrost peatlands (Joshi et al., 2021; Obradović et al., 2024), the available POM in our experiments could theoretically reduce 0.13 and 0.20 mmol Fe(III) in palsa and bog reactors, respectively (Table S6). As the actual amount of reduced Fe from added Fe(III)-OC coprecipitates was only 0.08 and 0.04 mmol after one day of incubation in palsa and bog soils, respectively, POM could have played a role in reducing Fe(III) in added coprecipitates. Overall, we therefore conclude that the rapid increase in aqueous Fe^{2+} originates from the microbially-induced reduction of added coprecipitates with a possible contribution of abiotic electron transfer from reduced POM to Fe(III).

4.2. Reduction of Fe(III)-OC coprecipitates in palsa and bog soils forms intermediate Fe(III)-OC phases

Besides the initial reduction of added Fe(III)-OC coprecipitates resulting in the increase in aqueous Fe^{2+}, there also was continued Fe (III) reduction in the solid phase. Results of XANES analysis indicated that there was less Fe(III) than expected due to the addition of coprecipitates (Fig. 2), indicating that a large proportion of coprecipitates was already reduced at the start of the experiment (49% and 37% for palsa and bog coprecipitates, respectively) before the sample for analysis by XAS (within 4 h) was taken. It is unlikely that we did not capture this fraction of coprecipitates due to a sampling bias, since the 0.5 M HCl extracted solids in the coprecipitate-amended treatments displayed the expected total content of Fe (30% of total Fe, Fig. S6d).

Further reduction of both added coprecipitates and native Fe(III) minerals occurred faster in the palsa soil than in bog soil. The reason might be higher DOC concentrations in palsa than in bog soil (Fig. S6g), specifically higher concentrations of substrates commonly serving as electron donors for Fe(III) reduction (Dong et al., 2023) like acetate or glucose (Fig. S14) (Coates et al., 1996; Küsel et al., 1999). The high DOC concentrations could have also led to more electron shuttling between the Fe(III)-OC coprecipitates and Fe(III)-reducers (Klüpfel et al., 2014; Scott et al., 1998). Further, the pH in palsa microcosms was lower than in bog microcosms (palsa: pH 3.4–3.8, bog: pH 4.2–4.7, Fig. S6i), leading to a higher standard electron potential of the Fe^{3+}/Fe^{2+} redox couple (Gorski et al., 2016; Kappler et al., 2021) in palsa microcosms compared to bog microcosms. This could have increased the rate of Fe(III) reduction in the palsa soil compared to the bog soil. Overall, the XANES spectra show that Fe(III)-OC coprecipitates were fully reduced in the palsa soil within 42 days since the fraction of Fe(III) was lower in the coprecipitate-amended treatment compared to the respective non-amended control. In the bog soil, it is also very likely that all added coprecipitates were reduced based on the slightly lower fraction of Fe (III) in the coprecipitate-amended treatment compared to the control after 42 days.

During this reduction, we identified notable changes in the speciation of Fe(III). Generally, results based on EXAFS suggest that the added coprecipitates (in form of ferrihydrite) were intermediately transformed to poorly-soluble Fe(III)-OC phases (Fig. 2). We speculate that part of the reduced Fe from coprecipitates might have been bound to POM and subsequently oxidized by reduced redox-active POM functional groups (e.g., quinones), as was previously shown under anoxic conditions (Joshi et al., 2024). This process could have occurred faster in the palsa soil (1 day) than in the bog soil (>10 days) due to the lower pH values which make quinone reduction more thermodynamically favorable (Uchimiya and Stone, 2009). However, the exact processes responsible for Fe(III)-OC formation in a ternary system of aqueous Fe^{2+}, Fe(III) (oxyhydr)oxides and POM under anoxic conditions deserve further study. The Fe(III)-OC phase is likely subsequently microbially reduced over time, forming Fe(II)-OC phases. For the bog treatment, we did not observe a reduction of Fe(III)-OC phase within the time span of the experiment, since the coprecipitates (in form of ferrihydrite) were reduced at a lower rate and just depleted at the end of the experiment. The same general temporal trends of the fraction of ferrihydrite and Fe (III)-OC were visible in the non-amended controls of both soils, due to reduction of native Fe(III) phases.

4.3. Greenhouse gas emissions in palsa soils are dominated by increased CO_2 emissions due to Fe(III)-OC coprecipitate reduction

Within the palsa soil, we observed an increase in CO_2 emissions relative to the non-amended treatment (Fig. 3), which is in line with microbial Fe(III) reduction coupled to organic matter respiration. We calculated how much CO_2 would be produced directly from the reduction of Fe(III) based on redox stoichiometry (4 mol Fe(III) reduced per 1 mol CO_2 produced from oxidation of OC) (Küsel et al., 2008; Lipson et al., 2013). We found that 15–30% of the increase in CO_2 emissions relative to the non-amended control may be attributable directly to Fe (III) reduction of the coprecipitates. Based on the rapid reductive dissolution of coprecipitates within 1 day, we did not observe an accompanying pulse in CO_2 emissions in the same timeframe (Fig. S7). It is likely that the expected pulse in CO_2 (max. 3.61 μmol CO_2 g^{-1} soil) is within the variation of experimental triplicates and was masked by the adsorption of native DOC (Fig. S6h), which likely also decreased CO_2 emissions in the coprecipitate-amended setup. The difference in CO_2 emissions between the treatments at the end of the experiment could also stem from the release and respiration of all Fe-bound OC, which would explain, on average, 66% of this difference. However, as the addition of coprecipitated OC only contributed to 0.1% of total OC and 7% of DOC in the palsa reactors, it is questionable whether there was a preferential mineralization of the previously Fe-bound OC. It is also possible that the release of Fe-bound OC stimulated further reduction of native Fe(III) minerals (ThomasArrigo et al., 2024) or induced priming effects so that the native OC pool was mineralized to a higher extent. Recent work by ThomasArrigo et al. (2023) and Wang et al. (2024) support the latter argument, since they found that the release of previously Fe-coprecipitated glucuronic acid/glucose led to higher respiration of native OC in anoxic soils.

We did not detect any CH_4 release in palsa soils within 72 days of anoxic conditions (Fig. 3), including the incubation time before addition of coprecipitates. This is in line with the absence of identified methanogens in the palsa soil based on the 16S rRNA amplicon sequencing data (Fig. S10) and the RNA-based *mcrA* gene copy numbers, which were below the detection limit. Our results are thus similar to previous metagenomic studies which mentioned the low to negligible activity of methanogens in palsa soil (Ellenbogen et al., 2024; McCalley et al., 2014). Still, we did expect to measure CH_4 emissions after a certain time lag in palsa reactors due to the establishment of anoxic conditions and

since field-based flux measurements showed high net CH_4 emission after initial palsa collapse (Patzner et al., 2022). The fact that our results therefore differ from field measurements might mean that (i) longer anoxic periods are necessary to establish methanogenic conditions or (ii) CH_4 release during palsa collapse in the field likely stems from the contact with bog methanogen communities. Support for the latter argument is given by Knoblauch et al. (2018) who found no CH_4 emissions from a Siberian permafrost soil layer with no detectable *mcrA* gene copies after 7 years of incubation, until they added an inoculum from another soil layer which contained active methanogens.

4.4. Reduction of Fe(III)-OC coprecipitates induces no change on net CO_2 release in bog soils and temporarily inhibits CH_4 emissions

In comparison to the palsa soil, we did not detect any difference in cumulative CO_2 emissions in the bog treatments (Fig. 3). This was surprising since the reduction of Fe(III) from the added coprecipitates should have produced an additional 100 μmol CO_2 g^{-1} soil within the incubation, based on the stoichiometry mentioned in section 4.3. Therefore, there was likely a counteracting effect on CO_2 release. It is possible that the activity of microorganisms was suppressed by the addition of certain *Sphagnum*-derived compounds that were initially coprecipitated with Fe. Such compounds could be sphagnan, a pectin-like polysaccharide stemming from the cell wall of *Sphagnum* mosses, or soluble phenolic compounds, which have both been shown to inhibit microbial respiration in bogs (Cory et al., 2022; Hájek et al., 2011). Since both sphagnan and phenolic compounds are abundant in bog porewaters (AminiTabrizi et al., 2020; Freeman et al., 2004; Painter, 1991) and likely also in bog WEOM, they were likely bound to Fe(III) (oxyhydr)oxides during the coprecipitation synthesis (Chen et al., 2016). It has also been suggested that release of Fe-bound OC in non-permafrost *Sphagnum* peatlands decreased β-glucosidase activity (Wang et al., 2022), which is a central enzyme for carbon degradation (Ketudat Cairns and Esen, 2010).

The bog treatments showed continuous CH_4 emissions (Fig. 3). Differences between the coprecipitate-amended and the non-amended control were only present in the first part of the incubation from 0 to 12 days, when cumulative CH_4 emissions were lower in the coprecipitate-amended treatment. This might indicate suppression of methanogenesis due to reduction of the Fe(III) in the added coprecipitates. However, once the majority of Fe(III)-OC coprecipitates were reduced (after 10 days), CH_4 emissions increased again, reaching the same cumulative CH_4 emission as in the non-amended treatment. The release of coprecipitated OC could have also played a role in increasing CH_4 production since it could have served as an additional OC source for fermenting microorganisms, which provide substrates for methanogenesis.

The trends in DNA-based *mcrA* gene copies are in line with the temporary suppression of CH_4 emissions between 0 and 12 days since $\log_2$ FC values of *mcrA* copies were the lowest at 8 days, compared to the beginning and the end of the experiment. However, the RNA-based *mcrA* copy numbers did not match with our hypothesis that temporary inhibition of methanogenesis occurred at the beginning of the experiment. We speculate that the difference between the DNA- and RNA-based *mcrA* values might be due to varying activity of methanogen taxa compared to their abundance. Some methanogens are hypothesized to be more vulnerable to competition effects with Fe(III)-reducing microorganisms (acetoclastic and hydrogenotrophic methanogens) than others (methylotrophic methanogens) (Jørgensen, 2006; Liu and Whitman, 2008). Indeed, Ellenbogen et al. (2024) found that methylotrophic methanogens can make up 7–54% of the total methanogen activity in bog soil and that members of the order *Methanosarcinales* are capable of using methoxylated compounds for methanogenesis. In any case, it was apparent that the addition of Fe(III)-OC coprecipitates temporarily decreased CH_4 emissions due to suppression of methanogenesis.

4.5. Fermenting and organic carbon-degrading microorganisms are stimulated by Fe(III)-OC coprecipitate addition

We found shifts in abundance and potential activity of several microbial taxa over time (Fig. 4). There was a high abundance of *Acidobacteriota* in both soils. The presence of this phylum is typical in permafrost soils (Hultman et al., 2015; Waldrop et al., 2023; Woodcroft et al., 2018) since *Acidobacteriota* encompass a wide array of taxa capable of complex polysaccharide degradation as well as several fermentation pathways (Woodcroft et al., 2018). Its increasing relative abundance over time in palsa soils could indicate the increase of fermenting bacteria due to anoxia. Similarly, higher relative abundances of *Firmicutes* in the coprecipitate-amended palsa treatment compared to the respective control after 42 days points towards a likely higher activity of fermenting microorganisms in this treatment (Li et al., 2024). Since fermentation produces low-molecular weight OC compounds, such fatty acids, which are often further mineralized to CO_2, *Firmicutes* could have indirectly contributed to the higher CO_2 emissions in the coprecipitate-amended treatment. The higher RNA-based gene copy numbers of bacterial and archaeal 16S rRNA gene in the coprecipitate-amended palsa soil compared to the non-amended control at day 0 could signal a potential priming effect, induced by the release of previously Fe-bound OC, as discussed above.

Within the bog soil, the relative abundance of *Fibrobacterota*, a taxon generally known for containing (hemi-)cellulose-degraders (Ransom-Jones et al., 2012; Weimer, 2022), significantly increased in the coprecipitate-amended treatment compared to the respective non-amended control, which could hint at a higher OC degradation potential. The similar quantity of copy numbers of the bacterial and archaeal 16S gene between the two bog treatments is also consistent with the lack of difference in cumulative CO_2 emissions between the two treatments.

Based on ANCOM analysis, *Sphingomonas* was significantly enriched in the coprecipitate-amended treatment of both soils compared to the non-amended control. This genus is ubiquitous in soils and known for degradation of a wide range of OC compounds (Sood et al., 2021), including aromatic compounds (Kim et al., 1996; Zylstra and Kim, 1997). We therefore speculate that *Sphingomonas* could have been involved in decomposition of the aromatic-rich OC that was released from the coprecipitates, since these moieties are found to preferentially bind to Fe(III) (oxyhydr)oxides (Chen et al., 2014; Voggenreiter et al., 2024; X. Zhu et al., 2023). Other upregulated taxa based on ANCOM also included *Geobacteraceae* in the bog soil. This family includes well-known respiratory Fe(III)-reducers, such as *Geobacter* (Coates et al., 1996; Lovley et al., 2004), which were likely more abundant due to the higher supply of Fe(III) in form of coprecipitates.

4.6. Estimation of CO_2 release from reduction of Fe(III)-OC associations in low-lying permafrost areas

Our results have wider implications for future CO_2 emissions of Fe-rich, low-lying permafrost areas. These regions will likely see an increase in CO_2 emissions upon thaw-induced anoxia due to the reduction of their native Fe(III)-OC associations. Based on previously published data on Fe stocks in permafrost soils (52–638 g Fe m^{-2} in the upper 30 cm) (Lipson et al., 2013; Mu et al., 2016; Patzner et al., 2020) and a constant stoichiometry of reduced Fe to produced CO_2 (4:1), 23 to 286 Tg C could be released as CO_2 upon the dissolution of Fe(III)-OC associations in low-land tundra or boreal ecosystems (Table S7) (Hugelius et al., 2014; Nitzbon et al., 2024). Our data even suggests that the ratio of reduced Fe to produced CO_2 after initial permafrost thaw is closer to 1:1, meaning that more CO_2 than that calculated from theoretical stoichiometry could be released.

There is potential for refining these estimates. First, only a few studies report the Fe content of permafrost soils as stocks scaled to area of soil instead of soil mass (Lipson et al., 2013; Mu et al., 2016; Patzner

et al., 2020). Therefore, upscaling of Fe contents across permafrost areas is highly uncertain due to limited measurements. Second, widespread projected changes in water saturation of permafrost soils do not exist yet, but would be needed in order to constrain the area of permafrost soils which will likely turn anoxic. For now, we assumed that all low-lying permafrost soils (Hugelius et al., 2014; Nitzbon et al., 2024) will turn anoxic, which may be an overestimation. We therefore propose (i) that future studies should analyze Fe contents along C contents in permafrost soils across a variety of permafrost areas to assess the importance and heterogeneity of Fe(III)-OC associations, and (ii) that modelling of future water saturation based on changes in rainfall, evapotranspiration, and thawing of permafrost ice should be conducted for permafrost areas.

5. Conclusion

Our work demonstrates that mineral-bound OC in the form of Fe(III)-OC associations is not protected after permafrost thaw followed by the onset of anoxic conditions. The added Fe(III)-OC coprecipitates were fully reduced within several weeks in collapsed palsa soils. The reduction increased CO_2 emissions by 43 ± 16% compared to the non-amended control, due to the use of Fe(III) as an additional electron acceptor and likely by releasing Fe-bound OC to the aqueous phase and priming the use of native DOC. As a result, excess emitted CO_2 was three times higher than expected based on the reduction of added Fe(III) alone. A simplified calculation based on our results suggests that 23 to 287 Tg C may be released due to microbial reduction of Fe(III)-OC associations from previously oxic permafrost soils.

The added Fe(III)-OC coprecipitates were also fully reduced in the naturally anoxic bog soils. Contrary to expectations, there was no clear increase in CO_2 emissions, such that we could not assess the direct contribution of Fe(III)-OC coprecipitates to CO_2 release. This suggests that counteracting processes, possibly due to the unique OC composition in *Sphagnum*-dominated bogs played a role. Once permafrost soils have transitioned into anoxic bog-like wetlands, the reduction of Fe(III)-OC associations might therefore not lead to excess CO_2 release. The underlying processes for this observation are still unclear and deserve further research. Regarding CH_4 emissions, it was apparent that the reduction of Fe(III)-OC coprecipitates temporarily decreased emissions in the bog soil, as long as coprecipitates were still present. Since bog soils often experience periodic water table fluctuations (Breeuwer et al., 2009; Olefeldt et al., 2012), the content of Fe(III)-OC associations could be replenished by abiotic oxidation of dissolved Fe^{2+} and coprecipitation of Fe and OC, leading to initial suppression of methanogenesis during anoxic periods. Further, the formation of Fe(III)-OC phases after coprecipitate dissolution, likely associated with POM, could explain the high C:Fe ratios found in *Sphagnum*-dominated wetlands (Zhao et al., 2023) and increase the persistence of Fe(III) under anoxic conditions. Together, our results therefore show that Fe(III)-OC associations are no stable C sink during anoxic conditions in thawing permafrost soils, thereby affecting the GHG balance in diverging ways depending on the soil biogeochemical conditions.

CRediT authorship contribution statement

Eva Voggenreiter: Writing – original draft, Visualization, Methodology, Investigation, Formal analysis, Conceptualization. **Laurel ThomasArrigo:** Writing – review & editing, Formal analysis. **Joachim Kilian:** Writing – review & editing, Methodology, Formal analysis. **Daniel Straub:** Methodology, Formal analysis. **Maike Friedel:** Investigation, Formal analysis. **Mark Stahl:** Writing – review & editing, Resources, Formal analysis. **Andreas Kappler:** Writing – review & editing, Supervision, Funding acquisition, Conceptualization. **Prachi Joshi:** Writing – review & editing, Supervision, Methodology, Formal analysis, Conceptualization.

Data statement

All data displayed in the figures is available at Zenodo (https://doi.org/10.5281/zenodo.13693408). Raw sequencing data has been deposited at NCBI in the Sequence Read Archive (SRA) under BioProject accession number PRJNA1123917 (https://www.ncbi.nlm.nih.gov/bioproject/PRJNA1123917). The samples discussed here contain in their sample title "palsa" (SAMN41832446 - SAMN41832481) or "bog" (SAMN41832374 - SAMN41832409).

Funding sources

This work was funded by the German Research foundation (DFG, KA 1736/66-1). A.K. acknowledges infrastructural support by the DFG under Germany's Excellence Strategy, cluster of Excellence EXC2124, project ID 390838134. Beamtime was supported by SOLEIL (proposal nb: 20221355) and ELETTRA (proposal nb: 20225213).

Declaration of competing interest

The authors declare that they have no known competing financial interests or personal relationships that could have appeared to influence the work reported in this paper.

Acknowledgements

We would like to thank the Swedish Polar Research Secretariat and SITES for the support during the work done at the Abisko Scientific Research Station. We are especially grateful to Emily Pederson for her help in the organization of the field campaign. We are also thankful for Hayley Green for assistance in the laboratory and Katrin Wunsch, Ankita Chauhan and Marie Mollenkopf for assistance during the field work. We further thank Sören Drabesch and Marie Mollenkopf for helpful discussions on gas analysis and experiment design. We acknowledge SOLEIL (proposal nr. 20221355) and ELETTRA (proposal nr. 20225213) for the use of the synchrotron radiation facilities and thank Gautier Landrot (SAMBA beamline, SOLEIL) and Luca Olivi (XAFS beamline, ELETTRA) for their help during the synchrotron data collection. We thank Thomas Borch for providing the XAS spectra of Fe-OC references. Furthermore, we are grateful for the help provided by Tsz Ho Chiu for freeze-drying, Martina Bottaro and Laura Tenelanda-Osorio for ICP-MS analyses and Franziska Schädler for molecular biology analyses. Sequencing was supported by the Institute for Medical Microbiology and Hygiene (MGM) of the University of Tübingen. The graphical abstract was made using BioRender.com.

Appendix A. Supplementary data

Supplementary data to this article can be found online at https://doi.org/10.1016/j.soilbio.2025.109735.

References

AminiTabrizi, R., Wilson, R.M., Fudyma, J.D., Hodgkins, S.B., Heyman, H.M., Rich, V.I., et al., 2020. Controls on soil organic matter degradation and subsequent greenhouse gas emissions across a permafrost thaw gradient in northern Sweden. Front Earth Sci 8, 557961. https://doi.org/10.3389/feart.2020.557961.

Andresen, C.G., Lawrence, D.M., Wilson, C.J., McGuire, A.D., Koven, C., Schaefer, K., et al., 2020. Soil moisture and hydrology projections of the permafrost region – a model intercomparison. The Cryosphere 14, 445–459. https://doi.org/10.5194/tc-14-445-2020.

Apprill, A., McNally, S., Parsons, R., Weber, L., 2015. Minor revision to V4 region SSU rRNA 806R gene primer greatly increases detection of SAR11 bacterioplankton. Aquatic Microbial Ecology 75, 129–137. https://doi.org/10.3354/ame01753.

Barreto, M.S.C., Wani, R.P., Goranov, A.I., Sowers, T.D., Fischel, M., Douglas, T.A., et al., 2024. Carbon fate, iron dissolution, and molecular Characterization of dissolved organic matter in thawed Yedoma permafrost under varying redox conditions. Environ Sci Technol. https://doi.org/10.1021/acs.est.3c08219 acs.est.3c08219.

Bauer, I., Kappler, A., 2009. Rates and extent of reduction of Fe(III) compounds and O_2 by humic substances. Environ Sci Technol 43, 4902–4908. https://doi.org/10.1021/es900179s.

Blöthe, M., Akob, D.M., Kostka, J.E., Göschel, K., Drake, H.L., Küsel, K., 2008. pH gradient-induced heterogeneity of Fe(III)-Reducing microorganisms in coal Mining-associated lake sediments. Applied and Environmental Microbiology 74, 1019–1029. https://doi.org/10.1128/AEM.01194-07.

Breeuwer, A., Robroek, B.J.M., Limpens, J., Heijmans, M.M.P.D., Schouten, M.G.C., Berendse, F., 2009. Decreased summer water table depth affects peatland vegetation. Basic and Applied Ecology 10, 330–339. https://doi.org/10.1016/j.baae.2008.05.005.

Chen, J., Gu, B., Royer, R., Burgos, W., 2003. The roles of natural organic matter in chemical and microbial reduction of ferric iron. Sci Total Environ 307, 167–178. https://doi.org/10.1016/S0048-9697(02)00538-7.

Chen, C., Dynes, J.J., Wang, J., Sparks, D.L., 2014. Properties of Fe-organic matter associations via coprecipitation versus adsorption. Environ Sci Technol 48, 13751–13759. https://doi.org/10.1021/es503669u.

Chen, K.-Y., Chen, T.-Y., Chan, Y.-T., Cheng, C.-Y., Tzou, Y.-M., Liu, Y.-T., et al., 2016. Stabilization of natural organic matter by short-range-order iron Hydroxides. Environ Sci Technol 50, 12612–12620. https://doi.org/10.1021/acs.est.6b02793.

Chen, C., Hall, S.J., Coward, E., Thompson, A., 2020. Iron-mediated organic matter decomposition in humid soils can counteract protection. Nature Communications 11, 2255. https://doi.org/10.1038/s41467-020-16071-5.

Coates, J.D., Phillips, E.J., Lonergan, D.J., Jenter, H., Lovley, D.R., 1996. Isolation of Geobacter species from diverse sedimentary environments. Applied and Environmental Microbiology 62, 1531–1536. https://doi.org/10.1128/aem.62.5.1531-1536.1996.

Cory, A.B., Chanton, J.P., Spencer, R.G.M., Ogles, O.C., Rich, V.I., McCalley, C.K., et al., 2022. Quantifying the inhibitory impact of soluble phenolics on anaerobic carbon mineralization in a thawing permafrost peatland. PLoS One 17, e0252743. https://doi.org/10.1371/journal.pone.0252743.

Dong, H., Zeng, Q., Sheng, Y., Chen, C., Yu, G., Kappler, A., 2023. Coupled iron cycling and organic matter transformation across redox interfaces. Nature Reviews Earth & Environment 4, 659–673. https://doi.org/10.1038/s43017-023-00470-5.

Drake, H.L., Horn, M.A., Wüst, P.K., 2009. Intermediary ecosystem metabolism as a main driver of methanogenesis in acidic wetland soil. Environ Microbiol Rep 1, 307–318. https://doi.org/10.1111/j.1758-2229.2009.00050.x.

Ellenbogen, J.B., Borton, M.A., McGivern, B.B., Cronin, D.R., Hoyt, D.W., Freire-Zapata, V., et al., 2024. Methylotrophy in the Mire: direct and indirect routes for methane production in thawing permafrost. mSystems 9. https://doi.org/10.1128/msystems.00698-23, 00698-23.

Ernakovich, J.G., Lynch, L.M., Brewer, P.E., Calderon, F.J., Wallenstein, M.D., 2017. Redox and temperature-sensitive changes in microbial communities and soil chemistry dictate greenhouse gas loss from thawed permafrost. Biogeochemistry 134, 183–200. https://doi.org/10.1007/s10533-017-0354-5.

Eusterhues, K., Hädrich, A., Neidhardt, J., Küsel, K., Keller, T.F., Jandt, K.D., et al., 2014. Reduction of ferrihydrite with adsorbed and coprecipitated organic matter: microbial reduction by Geobacter bremensis vs. abiotic reduction by Na-dithionite. Biogeosciences 11, 4953–4966. https://doi.org/10.5194/bg-11-4953-2014.

Ewels, P.A., Peltzer, A., Fillinger, S., Patel, H., Alneberg, J., Wilm, A., et al., 2020. The nf-core framework for community-curated bioinformatics pipelines. Nature Biotechnology 38, 276–278. https://doi.org/10.1038/s41587-020-0439-x.

Farquharson, L.M., Romanovsky, V.E., Cable, W.L., Walker, D.A., Kokelj, S.V., Nicolsky, D., 2019. Climate change Drives widespread and rapid thermokarst development in very cold permafrost in the Canadian high arctic. Geophysical Research Letters 46, 6681–6689. https://doi.org/10.1029/2019GL082187.

Freeman, C., Ostle, N.J., Fenner, N., Kang, H., 2004. A regulatory role for phenol oxidase during decomposition in peatlands. Soil Biol Biochem 36, 1663–1667. https://doi.org/10.1016/j.soilbio.2004.07.012.

Friedrich, M.W., 2005. Methyl-coenzyme M reductase genes: unique functional Markers for methanogenic and anaerobic methane-oxidizing Archaea. Methods in Enzymology 397, 428–442. https://doi.org/10.1016/S0076-6879(05)97026-2. Elsevier.

Gentsch, N., Mikutta, R., Shibistova, O., Wild, B., Schnecker, J., Richter, A., et al., 2015. Properties and bioavailability of particulate and mineral-associated organic matter in Arctic permafrost soils, Lower Kolyma Region, Russia. European Journal of Soil Science 66, 722–734. https://doi.org/10.1111/ejss.12269.

Gentsch, N., Wild, B., Mikutta, R., Čapek, P., Diáková, K., Schrumpf, M., et al., 2018. Temperature response of permafrost soil carbon is attenuated by mineral protection. Glob Change Biol 24, 3401–3415. https://doi.org/10.1111/gcb.14316.

Glodowska, M., Schneider, M., Eiche, E., Kontny, A., Neumann, T., Straub, D., et al., 2021. Fermentation, methanotrophy and methanogenesis influence sedimentary Fe and as dynamics in As-affected aquifers in Vietnam. Sci Total Environ 779, 146501. https://doi.org/10.1016/j.scitotenv.2021.146501.

Gorski, C.A., Edwards, R., Sander, M., Hofstetter, T.B., Stewart, S.M., 2016. Thermodynamic Characterization of iron oxide–aqueous Fe^{2+} redox couples. Environ Sci Technol 50, 8538–8547. https://doi.org/10.1021/acs.est.6b02661.

Graham, D.E., Wallenstein, M.D., Vishnivetskaya, T.A., Waldrop, M.P., Phelps, T.J., Pfiffner, S.M., et al., 2012. Microbes in thawing permafrost: the unknown variable in the climate change equation. ISME J 6, 709–712. https://doi.org/10.1038/ismej.2011.163.

Gray, N.D., McCann, C.M., Christgen, B., Ahammad, S.Z., Roberts, J.A., Graham, D.W., 2014. Soil geochemistry confines microbial abundances across an arctic landscape; implications for net carbon exchange with the atmosphere. Biogeochemistry 120, 307–317. https://doi.org/10.1007/s10533-014-9997-7.

Hájek, T., Ballance, S., Limpens, J., Zijlstra, M., Verhoeven, J.T.A., 2011. Cell-wall polysaccharides play an important role in decay resistance of Sphagnum and actively depressed decomposition in vitro. Biogeochemistry 103, 45–57. https://doi.org/10.1007/s10533-010-9444-3.

Herndon, E.M., Yang, Z., Bargar, J., Janot, N., Regier, T.Z., Graham, D.E., et al., 2015. Geochemical drivers of organic matter decomposition in arctic tundra soils. Biogeochemistry 126, 397–414. https://doi.org/10.1007/s10533-015-0165-5.

Heron, G., Crouzet, C., Bourg, A.C., Christensen, T.H., 1994. Speciation of Fe (II) and Fe (III) in contaminated aquifer sediments using chemical extraction techniques. Environmental Science & Technology 28 (9), 1698–1705.

Hu, Z., McKenna, A.M., Wen, K., Zhang, B., Mao, H., Goual, L., et al., 2024. Controls of mineral Solubility on adsorption-induced molecular Fractionation of dissolved organic matter revealed by 21 T FT-ICR MS. Environ Sci Technol 58, 2313–2322. https://doi.org/10.1021/acs.est.3c08123.

Huang, W., Hall, S.J., 2017. Elevated moisture stimulates carbon loss from mineral soils by releasing protected organic matter. Nature Communications 8, 1774. https://doi.org/10.1038/s41467-017-01998-z.

Hugelius, G., Strauss, J., Zubrzycki, S., Harden, J.W., Schuur, E.A.G., Ping, C.-L., et al., 2014. Estimated stocks of circumpolar permafrost carbon with quantified uncertainty ranges and identified data gaps. Biogeosciences 11, 6573–6593. https://doi.org/10.5194/bg-11-6573-2014.

Hultman, J., Waldrop, M.P., Mackelprang, R., David, M.M., McFarland, J., Blazewicz, S. J., et al., 2015. Multi-omics of permafrost, active layer and thermokarst bog soil microbiomes. Nature 521, 208–212. https://doi.org/10.1038/nature14238.

Johansson, T., Malmer, N., Crill, P.M., Friborg, T., Åkerman, J.H., Mastepanov, M., et al., 2006. Decadal vegetation changes in a northern peatland, greenhouse gas fluxes and net radiative forcing. Glob Change Biol 12, 2352–2369. https://doi.org/10.1111/j.1365-2486.2006.01267.x.

Jørgensen, B.B., 2006. Bacteria and marine biogeochemistry. In: Schulz, H.D., Zabel, M. (Eds.), Mar. Geochem. Springer-Verlag, Berlin/Heidelberg, pp. 169–206. https://doi.org/10.1007/3-540-32144-6_5.

Jorgenson, M.T., Harden, J., Kanevskiy, M., O'Donnell, J., Wickland, K., Ewing, S., et al., 2013. Reorganization of vegetation, hydrology and soil carbon after permafrost degradation across heterogeneous boreal landscapes. Environmental Research Letters 8, 035017. https://doi.org/10.1088/1748-9326/8/3/035017.

Joshi, P., Schroth, M.H., Sander, M., 2021. Redox properties of peat particulate organic matter: quantification of electron accepting capacities and Assessment of electron transfer Reversibility. J Geophys Res Biogeosciences 126, e2021JG006329. https://doi.org/10.1029/2021JG006329.

Joshi, P., ThomasArrigo, L.K., Sawwa, D., Sauter, L., Kappler, A., 2024. Complexation by particulate organic matter Alters iron redox Behavior. ACS Earth and Space Chemistry 8, 310–322. https://doi.org/10.1021/acsearthspacechem.3c00288.

Juottonen, H., Galand, P.E., Yrjälä, K., 2006. Detection of methanogenic Archaea in peat: comparison of PCR primers targeting the mcrA gene. Research in Microbiology 157, 914–921. https://doi.org/10.1016/j.resmic.2006.08.006.

Kappler, A., Bryce, C., Mansor, M., Lueder, U., Byrne, J.M., Swanner, E.D., 2021. An evolving view on biogeochemical cycling of iron. Nature Reviews Microbiology. https://doi.org/10.1038/s41579-020-00502-7.

Ketudat Cairns, J.R., Esen, A., 2010. β-Glucosidases. Cellular and Molecular Life Sciences 67, 3389–3405. https://doi.org/10.1007/s00018-010-0399-2.

Kim, E., Aversano, P.J., Romine, M.F., Schneider, R.P., Zylstra, G.J., 1996. Homology between genes for aromatic hydrocarbon degradation in surface and deep-subsurface Sphingomonas strains. Applied and Environmental Microbiology 62, 1467–1470. https://doi.org/10.1128/aem.62.4.1467-1470.1996.

Kleber, M., Eusterhues, K., Keiluweit, M., Mikutta, C., Mikutta, R., Nico, P.S., 2015. Mineral–organic associations: formation, properties. Relevance in Soil Environments. Elsevier, pp. 1–140. https://doi.org/10.1016/bs.agron.2014.10.005.

Klüpfel, L., Piepenbrock, A., Kappler, A., Sander, M., 2014. Humic substances as fully regenerable electron acceptors in recurrently anoxic environments. Nature Geoscience 7, 195–200. https://doi.org/10.1038/ngeo2084.

Knoblauch, C., Beer, C., Liebner, S., Grigoriev, M.N., Pfeiffer, E.-M., 2018. Methane production as key to the greenhouse gas budget of thawing permafrost. Nature Climate Change 8, 309–312. https://doi.org/10.1038/s41558-018-0095-z.

Kostka, J.E., Luther, G.W., 1994. Partitioning and speciation of solid phase iron in saltmarsh sediments. Geochim Cosmochim Acta 58, 1701–1710. https://doi.org/10.1016/0016-7037(94)90531-2.

Küsel, K., Dorsch, T., Acker, G., Stackebrandt, E., 1999. Microbial reduction of Fe(III) in acidic sediments: Isolation of *Acidiphilium cryptum* JF-5 capable of coupling the reduction of Fe(III) to the oxidation of glucose. Applied and Environmental Microbiology 65, 3633–3640. https://doi.org/10.1128/AEM.65.8.3633-3640.1999.

Küsel, K., Blöthe, M., Schulz, D., Reiche, M., Drake, H.L., 2008. Microbial reduction of iron and porewater biogeochemistry in acidic peatlands. Biogeosciences 5, 1537–1549. https://doi.org/10.5194/bg-5-1537-2008.

Lau, M.P., Sander, M., Gelbrecht, J., Hupfer, M., 2015. Solid phases as important electron acceptors in freshwater organic sediments. Biogeochemistry 123, 49–61. https://doi.org/10.1007/s10533-014-0052-5.

Li, H., Peng, J., Weber, K.A., Zhu, Y., 2011. Phylogenetic diversity of Fe(III)-reducing microorganisms in rice paddy soil: enrichment cultures with different short-chain fatty acids as electron donors. Journal of Soils and Sediments 11, 1234–1242. https://doi.org/10.1007/s11368-011-0371-2.

Li, L., Qu, Z., Wang, B., Qu, D., 2017. Dynamics of the abundance and structure of metabolically active Clostridium community in response to glucose additions in flooded paddy soils: closely correlated with hydrogen production and Fe(III) reduction. Journal of Soils and Sediments 17, 1727–1740. https://doi.org/10.1007/s11368-016-1637-5.

Li, Y., Xue, Y., Roy Chowdhury, T., Graham, D.E., Tringe, S.G., Jansson, J.K., et al., 2024. Genomic insights into redox-driven microbial processes for carbon decomposition in thawing Arctic soils and permafrost. mSphere. https://doi.org/10.1128/msphere.00259-24, 00259-24.

Lim, A.G., Loiko, S.V., Pokrovsky, O.S., 2022. Sizable pool of labile organic carbon in peat and mineral soils of permafrost peatlands, western Siberia. Geoderma 409, 115601. https://doi.org/10.1016/j.geoderma.2021.115601.

Lipson, D.A., Jha, M., Raab, T.K., Oechel, W.C., 2010. Reduction of iron (III) and humic substances plays a major role in anaerobic respiration in an Arctic peat soil. Journal of Geophysical Research 115. https://doi.org/10.1029/2009JG001147.

Lipson, D.A., Zona, D., Raab, T.K., Bozzolo, F., Mauritz, M., Oechel, W.C., 2012. Water-table height and microtopography control biogeochemical cycling in an Arctic coastal tundra ecosystem. Biogeosciences 9, 577–591. https://doi.org/10.5194/bg-9-577-2012.

Lipson, D.A., Raab, T.K., Goria, D., Zlamal, J., 2013. The contribution of Fe(III) and humic acid reduction to ecosystem respiration in drained thaw lake basins of the Arctic Coastal Plain. Glob Biogeochem Cycles 27, 399–409. https://doi.org/10.1002/gbc.20038.

Liu, Y., Whitman, W.B., 2008. Metabolic, Phylogenetic, and Ecological diversity of the methanogenic Archaea. Annals of the New York Academy of Sciences 1125, 171–189. https://doi.org/10.1196/annals.1419.019.

Liu, F., Qin, S., Fang, K., Chen, L., Peng, Y., Smith, P., et al., 2022. Divergent changes in particulate and mineral-associated organic carbon upon permafrost thaw. Nature Communications 13, 5073. https://doi.org/10.1038/s41467-022-32681-7.

Lovley, D.R., Holmes, D.E., Nevin, K.P., 2004. Dissimilatory Fe(III) and Mn(IV) reduction. Advances in Microbial Physiology 212–286.

Malmer, N., Johansson, T., Olsrud, M., Christensen, T.R., 2005. Vegetation, climatic changes and net carbon sequestration in a North-Scandinavian subarctic mire over 30 years. Glob Change Biol 0, 051006062331004. https://doi.org/10.1111/j.1365-2486.2005.01042.x.

Mandal, S., Van Treuren, W., White, R.A., Eggesbø, M., Knight, R., Peddada, S.D., 2015. Analysis of composition of microbiomes: a novel method for studying microbial composition. Microbial Ecology in Health and Disease 26. https://doi.org/10.3402/mehd.v26.27663.

Martens, J., Mueller, C.W., Joshi, P., Rosinger, C., Maisch, M., Kappler, A., et al., 2023. Stabilization of mineral-associated organic carbon in Pleistocene permafrost. Nature Communications 14, 2120. https://doi.org/10.1038/s41467-023-37766-5.

McCalley, C.K., Woodcroft, B.J., Hodgkins, S.B., Wehr, R.A., Kim, E.-H., Mondav, R., et al., 2014. Methane dynamics regulated by microbial community response to permafrost thaw. Nature 514, 478–481. https://doi.org/10.1038/nature13798.

Miller, K.E., Lai, C.-T., Friedman, E.S., Angenent, L.T., Lipson, D.A., 2015. Methane suppression by iron and humic acids in soils of the Arctic Coastal Plain. Soil Biol Biochem 83, 176–183. https://doi.org/10.1016/j.soilbio.2015.01.022.

Monhonval, A., Strauss, J., Thomas, M., Hirst, C., Titeux, H., Louis, J., et al., 2022. Thermokarst processes increase the supply of stabilizing surfaces and elements (Fe, Mn, Al, and Ca) for mineral–organic carbon interactions. Permafrost and Periglacial Processes 33, 452–469. https://doi.org/10.1002/ppp.2162.

Monhonval, A., Hirst, C., Strauss, J., Schuur, E.A.G., Opfergelt, S., 2023a. Strontium isotopes trace the dissolution and precipitation of mineral organic carbon interactions in thawing permafrost. Geoderma 433, 116456. https://doi.org/10.1016/j.geoderma.2023.116456.

Monhonval, A., Mauclet, E., Hirst, C., Bemelmans, N., Eekman, E., Schuur, E.A.G., et al., 2023b. Mineral organic carbon interactions in dry versus wet tundra soils. Geoderma 436, 116552. https://doi.org/10.1016/j.geoderma.2023.116552.

Mu, C.C., Zhang, T.J., Zhao, Q., Guo, H., Zhong, W., Su, H., et al., 2016. Soil organic carbon stabilization by iron in permafrost regions of the Qinghai-Tibet Plateau. Geophysical Research Letters 43, 10286–10294. https://doi.org/10.1002/2016GL070071.

Nitzbon, J., Schneider Von Deimling, T., Aliyeva, M., Chadburn, S.E., Grosse, G., Laboor, S., et al., 2024. No respite from permafrost-thaw impacts in the absence of a global tipping point. Nature Climate Change 14, 573–585. https://doi.org/10.1038/s41558-024-02011-4.

Notini, L., ThomasArrigo, L.K., Kaegi, R., Kretzschmar, R., 2022. Coexisting Goethite promotes Fe(II)-Catalyzed transformation of ferrihydrite to Goethite. Environ Sci Technol 56, 12723–12733. https://doi.org/10.1021/acs.est.2c03925.

Obradović, N., Schmitz, R.A., Haffter, F., Meier, D.V., Lever, M.A., Schroth, M.H., et al., 2024. Peat particulate organic matter Accepts electrons during in situ incubation in the anoxic subsurface of Ombrotrophic bogs. J Geophys Res Biogeosciences 129, e2024JG008223. https://doi.org/10.1029/2024JG008223.

Olefeldt, D., Roulet, N.T., Bergeron, O., Crill, P., Bäckstrand, K., Christensen, T.R., 2012. Net carbon accumulation of a high-latitude permafrost palsa mire similar to permafrost-free peatlands. Geophysical Research Letters 39. https://doi.org/10.1029/2011GL050355.

Painter, T.J., 1991. Lindow man, tollund man and other peat-bog bodies: the preservative and antimicrobial action of Sphagnan, a reactive glycuronoglycan with tanning and sequestering properties. Carbohydrate Polymers 15, 123–142. https://doi.org/10.1016/0144-8617(91)90028-B.

Parada, A.E., Needham, D.M., Fuhrman, J.A., 2016. Every base matters: assessing small subunit rRNA primers for marine microbiomes with mock communities, time series and global field samples. Environmental Microbiology 18, 1403–1414. https://doi.org/10.1111/1462-2920.13023.

Patzner, M.S., Mueller, C.W., Malusova, M., Baur, M., Nikeleit, V., Scholten, T., et al., 2020. Iron mineral dissolution releases iron and associated organic carbon during permafrost thaw. Nature Communications 11, 6329. https://doi.org/10.1038/s41467-020-20102-6.

Patzner, M.S., Logan, M., McKenna, A.M., Young, R.B., Zhou, Z., Joss, H., et al., 2022. Microbial iron cycling during palsa hillslope collapse promotes greenhouse gas emissions before complete permafrost thaw. Commun Earth Environ 3. https://doi.org/10.1038/s43247-022-00407-8.

Pedersen, H.D., Postma, D., Jakobsen, R., Larsen, O., 2005. Fast transformation of iron oxyhydroxides by the catalytic action of aqueous Fe(II). Geochim Cosmochim Acta 69, 3967–3977. https://doi.org/10.1016/j.gca.2005.03.016.

Poggenburg, C., Mikutta, R., Schippers, A., Dohrmann, R., Guggenberger, G., 2018. Impact of natural organic matter coatings on the microbial reduction of iron oxides. Geochim Cosmochim Acta 224, 223–248. https://doi.org/10.1016/j.gca.2018.01.004.

R Core Team, 2024. R: A Language and Environment for Statistical Computing.

Ransom-Jones, E., Jones, D.L., McCarthy, A.J., McDonald, J.E., 2012. The Fibrobacteres: an important phylum of cellulose-degrading bacteria. Microbial Ecology 63, 267–281. https://doi.org/10.1007/s00248-011-9998-1.

Ravel, B., Newville, M., 2005. ATHENA and ARTEMIS Interactive graphical data Analysisusing IFEFFIT. Phys Scr 2005, 1007. https://doi.org/10.1238/Physica.Topical.115a01007.

Reiche, M., Torburg, G., Küsel, K., 2008. Competition of Fe(III) reduction and methanogenesis in an acidic fen. FEMS Microbiology Ecology 65, 88–101. https://doi.org/10.1111/j.1574-6941.2008.00523.x.

Roden, E.E., Kappler, A., Bauer, I., Jiang, J., Paul, A., Stoesser, R., et al., 2010. Extracellular electron transfer through microbial reduction of solid-phase humic substances. Nature Geoscience 3, 417–421. https://doi.org/10.1038/ngeo870.

Schuur, E.A.G., McGuire, A.D., Schädel, C., Grosse, G., Harden, J.W., Hayes, D.J., et al., 2015. Climate change and the permafrost carbon feedback. Nature 520, 171–179. https://doi.org/10.1038/nature14338.

Schuur, E.A.G., Abbott, B.W., Commane, R., Ernakovich, J., Euskirchen, E., Hugelius, G., et al., 2022. Permafrost and climate change: carbon cycle feedbacks from the warming arctic. Annual Review of Environment and Resources 47, 343–371. https://doi.org/10.1146/annurev-environ-012220-011847.

Scott, D.T., McKnight, D.M., Blunt-Harris, E.L., Kolesar, S.E., Lovley, D.R., 1998. Quinone moieties Act as electron acceptors in the reduction of humic substances by Humics-reducing microorganisms. Environ Sci Technol 32, 2984–2989. https://doi.org/10.1021/es980272q.

Sim, T.G., Swindles, G.T., Morris, P.J., Baird, A.J., Cooper, C.L., Gallego-Sala, A.V., et al., 2021. Divergent responses of permafrost peatlands to recent climate change. Environmental Research Letters 16, 034001. https://doi.org/10.1088/1748-9326/abe00b.

Sood, U., Hira, P., Singh, P., Singh, D.N., Lal, R., 2021. Sphingomonas. In: Whitman, W.B. (Ed.), Bergeys Man. Syst. Archaea Bact, first ed. Wiley, pp. 1–84. https://doi.org/10.1002/9781118960608.gbm00924.pub2.

Stookey, L.L., 1970. Ferrozine—a new spectrophotometric reagent for iron. Analytical Chemistry 42, 779–781. https://doi.org/10.1021/ac60289a016.

Straub, D., Blackwell, N., Langarica-Fuentes, A., Peltzer, A., Nahnsen, S., Kleindienst, S., 2020. Interpretations of environmental microbial community studies are biased by the selected 16S rRNA (gene) amplicon sequencing Pipeline. Frontiers in Microbiology 11, 550420. https://doi.org/10.3389/fmicb.2020.550420.

Straub, D., Tångrot, J., Peltzer, A., Lundin, D., 2024. nf-core/ampliseq: ampliseq Version 2.8.0. emnilsson, nf-core bot, et al. https://doi.org/10.5281/ZENODO.1493841.

Sun, F.-S., Ma, C., Yu, G.-H., Kuzyakov, Y., Lang, Y.-C., Fu, P.-Q., et al., 2023. Organic carbon preservation in wetlands: iron oxide protection vs. thermodynamic limitation. Water Research 241, 120133. https://doi.org/10.1016/j.watres.2023.120133.

Swedish Meteorological and Hydrological Institute, 2020. Air temperature, Abisko station. https://www.smhi.se/data/meteorologi/ladda-ner-meteorologiska-observationer#stationid=188800,param=airtemperatureInstant,stations=core.

Thomas, M., Monhonval, A., Hirst, C., Bröder, L., Zolkos, S., Vonk, J.E., et al., 2023. Evidence for preservation of organic carbon interacting with iron in material displaced from retrogressive thaw slumps: case study in Peel Plateau, western Canadian Arctic. Geoderma 433, 116443. https://doi.org/10.1016/j.geoderma.2023.116443.

Thomas, M., Jongejans, L.L., Strauss, J., Vermylen, C., Calcus, S., Opel, T., et al., 2024. A third of organic carbon is mineral bound in permafrost sediments exposed by the World's largest thaw Slump, Batagay, Siberia. Permafrost and Periglacial Processes 2230. https://doi.org/10.1002/ppp.2230.

ThomasArrigo, L.K., Mikutta, C., Byrne, J., Kappler, A., Kretzschmar, R., 2017. Iron(II)-Catalyzed iron Atom exchange and Mineralogical changes in iron-rich organic freshwater Flocs: an iron isotope tracer study. Environ Sci Technol 51, 6897–6907. https://doi.org/10.1021/acs.est.7b01495.

ThomasArrigo, L.K., Byrne, J.M., Kappler, A., Kretzschmar, R., 2018. Impact of organic matter on iron(II)-Catalyzed mineral transformations in ferrihydrite-organic matter coprecipitates. Environ Sci Technol 52, 12316–12326. https://doi.org/10.1021/acs.est.8b03206.

ThomasArrigo, L.K., Vontobel, S., Notini, L., Nydegger, T., 2023. Coprecipitation with ferrihydrite inhibits mineralization of glucuronic acid in an anoxic soil. Environ Sci Technol 57, 9204–9213. https://doi.org/10.1021/acs.est.3c01336.

ThomasArrigo, L.K., Notini, L., Vontobel, S., Bouchet, S., Nydegger, T., Kretzschmar, R., 2024. Emerging investigator series: coprecipitation with glucuronic acid limits reductive dissolution and transformation of ferrihydrite in an anoxic soil. Environ Sci Process Impacts. https://doi.org/10.1039/D4EM00238E, 10.1039.D4EM00238E.

Treude, N., Rosencrantz, D., Liesack, W., Schnell, S., 2003. Strain FAc12, a dissimilatory iron-reducing member of the Anaeromyxobacter subgroup of Myxococcales. FEMS Microbiology Ecology 44, 261–269. https://doi.org/10.1016/S0168-6496(03)00048-5.

Turetsky, M.R., Abbott, B.W., Jones, M.C., Anthony, K.W., Olefeldt, D., Schuur, E.A.G., et al., 2020. Carbon release through abrupt permafrost thaw. Nature Geoscience 13, 138–143. https://doi.org/10.1038/s41561-019-0526-0.

Uchimiya, M., Stone, A.T., 2009. Reversible redox chemistry of quinones: impact on biogeochemical cycles. Chemosphere 77, 451–458. https://doi.org/10.1016/j.chemosphere.2009.07.025.

Varner, R.K., Crill, P.M., Frolking, S., McCalley, C.K., Burke, S.A., Chanton, J.P., et al., 2022. Permafrost thaw driven changes in hydrology and vegetation cover increase trace gas emissions and climate forcing in Stordalen Mire from 1970 to 2014. Philos Transact A Math Phys Eng Sci 380, 20210022. https://doi.org/10.1098/rsta.2021.0022.

Voggenreiter, E., Schmitt-Kopplin, P., ThomasArrigo, L., Bryce, C., Kappler, A., Joshi, P., 2024. Emerging investigator series: preferential adsorption and coprecipitation of permafrost organic matter with poorly crystalline iron minerals. Environ Sci Process Impacts. https://doi.org/10.1039/D4EM00241E, 10.1039.D4EM00241E.

Waldrop, M.P., Chabot, C.L., Liebner, S., Holm, S., Snyder, M.W., Dillon, M., et al., 2023. Permafrost microbial communities and functional genes are structured by latitudinal and soil geochemical gradients. ISME J 17, 1224–1235. https://doi.org/10.1038/s41396-023-01429-6.

Walter Anthony, K., Schneider Von Deimling, T., Nitze, I., Frolking, S., Emond, A., Daanen, R., et al., 2018. 21st-century modeled permafrost carbon emissions accelerated by abrupt thaw beneath lakes. Nature Communications 9, 3262. https://doi.org/10.1038/s41467-018-05738-9.

Wang, Y., Liu, X., Zhang, X., Dai, G., Wang, Z., Feng, X., 2022. Evaluating wetland soil carbon stability related to iron transformation during redox oscillations. Geoderma 428, 116222. https://doi.org/10.1016/j.geoderma.2022.116222.

Wang, S., Gao, W., Ma, Z., Zhu, Z., Luo, Y., Wei, L., et al., 2024. Iron mineral type controls organic matter stability and priming in paddy soil under anaerobic conditions. Soil Biol Biochem, 109518. https://doi.org/10.1016/j.soilbio.2024.109518.

Weimer, P.J., 2022. Degradation of cellulose and Hemicellulose by Ruminal microorganisms. Microorganisms 10, 2345. https://doi.org/10.3390/microorganisms10122345.

Williams, A.G.B., Scherer, M.M., 2004. Spectroscopic evidence for Fe(II)−Fe(III) electron transfer at the iron Oxide−Water Interface. Environ Sci Technol 38, 4782–4790. https://doi.org/10.1021/es049373g.

Winkel, M., Mitzscherling, J., Overduin, P.P., Horn, F., Winterfeld, M., Rijkers, R., et al., 2018. Anaerobic methanotrophic communities thrive in deep submarine permafrost. Scientific Reports 8, 1291. https://doi.org/10.1038/s41598-018-19505-9.

Woo, M., Young, K.L., 2006. High Arctic wetlands: their occurrence, hydrological characteristics and sustainability. J Hydrol 320, 432–450. https://doi.org/10.1016/j.jhydrol.2005.07.025.

Woodcroft, B.J., Singleton, C.M., Boyd, J.A., Evans, P.N., Emerson, J.B., Zayed, A.A.F., et al., 2018. Genome-centric view of carbon processing in thawing permafrost. Nature 560, 49–54. https://doi.org/10.1038/s41586-018-0338-1.

Yang, Z., Wullschleger, S.D., Liang, L., Graham, D.E., Gu, B., 2016. Effects of warming on the degradation and production of low-molecular-weight labile organic carbon in an Arctic tundra soil. Soil Biol Biochem 95, 202–211. https://doi.org/10.1016/j.soilbio.2015.12.022.

Zhao, B., Dou, A., Zhang, Z., Chen, Z., Sun, W., Feng, Y., 2023a. Ecosystem-specific patterns and drivers of global reactive iron mineral-associated organic carbon. Biogeosciences 20, 4761–4774. https://doi.org/10.5194/bg-20-4761-2023.

Zhao, Y., Liu, C., Li, X., Ma, L., Zhai, G., Feng, X., 2023b. Sphagnum increases soil's sequestration capacity of mineral-associated organic carbon via activating metal oxides. Nature Communications 14, 5052. https://doi.org/10.1038/s41467-023-40863-0.

Zhu, E., Liu, Z., Wang, S., Wang, Y., Liu, T., Feng, X., 2023a. Organic carbon and Lignin protection by metal oxides versus Silicate Clay: Comparative study based on wetland and Upland soils. J Geophys Res Biogeosciences 128, e2023JG007474. https://doi.org/10.1029/2023JG007474.

Zhu, X., Wang, K., Liu, Z., Wang, J., Wu, E., Yu, W., et al., 2023b. Probing molecular-level Dynamic interactions of dissolved organic matter with iron Oxyhydroxide via a coupled Microfluidic reactor and an online high-Resolution mass spectrometry system. Environ Sci Technol 57, 2981–2991. https://doi.org/10.1021/acs.est.2c06816.

Zylstra, G.J., Kim, E., 1997. Aromatic hydrocarbon degradation by Sphingomonas yanoikuyae B1. J Ind Microbiol Biotechnol 19, 408–414. https://doi.org/10.1038/sj.jim.2900475.